

AperTO - Archivio Istituzionale Open Access dell'Università di Torino

mGluR5 PAMs rescue cortical and behavioural defects in a mouse model of CDKL5 deficiency disorder

This is a pre print version of the following article:

Original Citation:

Availability:

This version is available <http://hdl.handle.net/2318/1876730> since 2022-10-18T11:40:43Z

Published version:

DOI:10.1038/s41386-022-01412-3

Terms of use:

Open Access

Anyone can freely access the full text of works made available as "Open Access". Works made available under a Creative Commons license can be used according to the terms and conditions of said license. Use of all other works requires consent of the right holder (author or publisher) if not exempted from copyright protection by the applicable law.

(Article begins on next page)

1 **mGluR5 PAMs rescue cortical and behavioural defects in a mouse model of**
2 **CDKL5 deficiency disorder.**

3 Antonia Gurgone¹, Riccardo Pizzo¹, Alessandra Raspanti¹, Giuseppe Chiantia¹, Sunaina Devi¹,
4 Noemi Morello¹, Federica Pilotto¹, Sara Gnavi¹, Leonardo Lupori², Raffaele Mazziotti³, Giulia
5 Sagona³, Elena Putignano⁴, Alessio Nocentini⁵, Claudiu T. Supuran⁵, Andrea Marcantoni⁶, Tommaso
6 Pizzorusso^{2,4} and Maurizio Giustetto^{1*}

7 ¹Rita Levi-Montalcini” Department of Neuroscience, University of Turin, Turin (Italy); ²BIO@SNS
8 lab, Scuola Normale Superiore, 56124 Pisa, Italy; ³Department of Developmental Neuroscience,
9 IRCCS Stella Maris Foundation, 56128 Pisa, Italy, ⁴Institute of Neuroscience, CNR, 56124 Pisa,
10 Italy; ⁵NEUROFARBA Department, Section of Pharmaceutical and Nutraceutical Sciences,
11 University of Florence, 50019 Sesto Fiorentino (Florence), Italy. ⁶Department of Drug Science,
12 University of Turin, Turin, Italy.

13

14

15 *Correspondence: maurizio.giustetto@unito.it

16 Università di Torino, Dipartimento di Neuroscienze “Rita Levi Montalcini”

17 Corso Raffaello 30; 10125 Torino – ITALY

18 Tel. +39-011-670-7725 (office); +39-011-670-7731 (lab)

19

20 **Abstract**

21 Cyclin-dependent kinase-like 5 (CDKL5) deficiency disorder (CDD) is a devastating rare
22 neurodevelopmental disease without a cure, caused by mutations of the serine/threonine kinase
23 CDKL5 highly expressed in the forebrain. CDD is characterized by early-onset seizures, severe
24 intellectual disabilities, autistic-like traits, sensorimotor and cortical visual impairments (CVI). The
25 lack of an effective therapeutic strategy for CDD urgently demands the identification of novel
26 druggable targets potentially relevant for CDD pathophysiology.

27 To this aim, we studied metabotropic glutamate receptors 5 (mGluR5) for their important role in
28 critical mechanisms involved in CDD, i.e.: synaptogenesis, dendritic spines formation/maturation and
29 synaptic plasticity, and because mGluR5 function depends on the postsynaptic protein Homer1bc that
30 is downregulated in the cerebral cortex of CDKL5^{-y} mice. In this study, we reveal that CDKL5 loss
31 tampers with (i) the strength of Homer1bc-mGluR5 binding, (ii) the synaptic localization of mGluR5
32 and (iii) the mGluR5-mediated enhancement of NMDA-induced neuronal responses. Importantly, we
33 showed that the stimulation of mGluR5 activity by administering in mice specific positive-allosteric-
34 modulators, i.e.: 3-Cyano-N-(1,3-diphenyl-1H-pyrazol-5-yl)benzamide (CDPPB) or RO6807794,
35 corrected the synaptic, functional and behavioural defects shown by CDKL5^{-y} mice. Notably, the
36 cerebral cortex of 2 CDD patients show similar changes in the synaptic organization to mutant
37 CDKL5 mice, including a reduced mGluR5 expression, suggesting that mGluR5 represent a
38 promising therapeutic target for CDD patients.

39

40 **Keywords:** neurodevelopmental disorders; synapses; NMDA-mediated current; synaptic
41 transmission; cerebral cortex

42

43 **1. Introduction**

44 CDKL5 is a serine/threonine kinase highly expressed especially in the forebrain during the peak of
45 synaptogenesis (Rusconi et al., 2008). CDKL5 phosphorylates several substrates and is involved in a
46 broad variety of cellular processes such as gene expression, neuronal migration, axon outgrowth,
47 dendritic morphogenesis, synapses development and function (Baltussen et al., 2018; Muñoz et al.,
48 2018; Nawaz et al., 2016; Trazzi et al., 2016). In the nucleus CDKL5 has been shown to interact with
49 epigenetic factors, such as methyl-CpG-binding protein 2 (MeCP2) and DNA Methyltransferase 1
50 (DNMT1) (Kameshita et al., 2008; Mari et al., 2005), nevertheless the role of CDKL5 in regulating
51 gene expression is still not fully understood. Recently, several cytoplasmic targets of CDKL5
52 phosphorylation, including MAP1S, EB2 and ARHGEF2, have been identified pointing to a major
53 role of this kinase in the control of cytoskeletal function. Moreover, CDKL5 has been found to
54 accumulate at synapses where it can interact with the palmitoylated form of postsynaptic density
55 protein-95 (PSD-95) (Zhu et al., 2013). The interaction with PSD95 facilitates the phosphorylation
56 of the adhesion molecule netrin-G1 ligand (NGL-1) (Ricciardi et al., 2012) promoting the maturation
57 of dendritic spines, i.e., the vast majority of glutamatergic postsynaptic sites in the forebrain, as well
58 as the formation and function of excitatory connections. In addition, Barbiero et al. (2017) (Barbiero
59 et al., 2017) showed that IQ motif containing GTPase activating protein 1 (IQGAP1) can interact with
60 CDKL5 and thus mediate the formation of complexes with post-synaptic proteins such as PSD-95 or
61 both AMPA- and NMDA-glutamatergic receptors. Interestingly, shRNA-mediated knockdown of
62 CDKL5 can influence the synaptic expression of the GluA2 subunit (Tramarin et al., 2018) further
63 highlighting that the involvement of CDKL5 in glutamatergic neurotransmission is yet to be unfolded.

64 To study the consequences of the lack of CDKL5 *in-vivo*, different CDKL5^{-y} mouse lines have been
65 recently generated (Amendola et al., 2014; Okuda et al., 2017; Wang et al., 2012). They all display a
66 broad spectrum of behavioural abnormalities, including hind-limb claspings, motor hyperactivity,
67 abnormal eye tracking, learning and memory deficits, and autistic-like phenotypes (Okuda et al.,

68 2017), closely modelling human CDD (Demarest et al., 2019). Moreover, sensory defects such as
69 tactile, visual and auditory impairments were recently revealed in CDD mouse models (Mazziotti et
70 al., 2017; Pizzo et al., 2019; Wang et al., 2012). For example, cortical visual impairment (CVI), that
71 is correlated with developmental delay in CDD patients (Demarest et al., 2019), is found in CDKL5
72 mutant mice starting from P27-P28 both in heterozygous and homozygous animals (Mazziotti et al.,
73 2017; Wang et al., 2012).

74 Aberrant sensory processing in mice lacking CDKL5 is associated with severe abnormalities of the
75 cerebral cortex, including altered dendritic arborization of pyramidal neurons, the downregulation of
76 the postsynaptic scaffolding proteins PSD-95 and Homer, and the disruption of AKT-mTOR
77 signaling (Amendola et al., 2014; Della Sala et al., 2016; Lupori et al., 2019; Pizzo et al., 2016; Wang
78 et al., 2012). Moreover, we reported previously that CDKL5 plays a key role in the dynamic of
79 dendritic spines turn-over in the primary somatosensory (S1) cortex (Della Sala et al., 2016) by
80 promoting their stabilization. In addition, S1 cortex of CDKL5^{-y} mice show impaired excitatory
81 synaptic transmission and maintenance of long-term potentiation induced by theta-burst stimulation,
82 emphasizing the role of CDKL5 in excitatory cortical connectivity (Della Sala et al., 2016; Pizzo et
83 al., 2019).

84 Given all the above, we reasoned that by identifying druggable targets with relevant synaptic function
85 is of pivotal importance to uncover novel therapeutic options for CDD. Here we report that both the
86 expression and function of a member of group I metabotropic glutamate receptors, mGluR5, are
87 abnormal in CDKL5^{-y} mice cerebral cortex and that the administration of selective mGluR5 positive
88 allosteric modulators (PAMs) can rescue synaptic, cellular, and behavioural defects shown by mutant
89 mice.

90

91

92 **2. Results**

93 ***2.1. Altered mGluR5/Homer1bc organization in the cerebral cortex of Cdk15^{-y} mice.***

94 We focused the analyses on mGluR5 guided by mounting evidence pointing at their role in critical
95 mechanisms involved in CDD such as synaptogenesis, dendritic spines formation/maturation and
96 synaptic plasticity (Ballester-Rosado et al., 2016; Chen et al., 2012; Edfawy et al., 2019; Piers et al.,
97 2012). mGluR5 needs to interact with Homer1bc to exert its signaling functions within the PSD
98 (Giuffrida et al., 2005; Ronesi et al., 2012; Scheefhals and MacGillavry, 2018; Tu et al., 1999). Since
99 Homer1bc is downregulated in the cortex of CDKL5^{-y} mice (Pizzo et al., 2019, 2016), we evaluated
100 the strength of mGluR5-Homer1bc binding in mutant mice. Intriguingly, co-immunoprecipitation
101 (co-IP) assays of cortical synaptosomal fraction (fig.1A) revealed that the amount of mGluR5
102 immunoprecipitated with Homer1bc is significantly reduced in Cdk15^{-y} mice compared to Cdk15^{+y}
103 animals (O.D mGluR5/Homer1bc * $p < 0.05$; fig 1B). We next assessed mGluR5 expression in the
104 neuropil by performing immunofluorescence experiments on S1 cortices from Cdk15^{-y} and Cdk15^{+y}
105 mice (fig. 1C). By using a fixation/staining protocol improved for postsynaptic protein localization
106 (Morello et al., 2018; Pizzo et al., 2016), mGluR5 immunofluorescence (fig. 1C) resulted in discrete
107 puncta that were found closely localized, but only rarely overlapping, with PSD-95⁺ puncta in
108 agreement with previously reported perisynaptic localization of mGluR5 (Lujan et al., 1996).
109 Interestingly, the quantitative analysis (fig. 1D) revealed that mGluR5-puncta density is strongly
110 reduced in layers II-III and V of somatosensory (S1) cortex in Cdk15^{-y} mice compared to controls
111 (layers II-III and layer V: Cdk15^{+y} vs Cdk15^{-y} * $p < 0.05$; fig. 1C-D). These findings indicate that the
112 presence of CDKL5 is required for both mGluR5-Homer1bc binding and the synaptic localization of
113 mGluR5.

114

115

116

117 **2.2 mGluR5-mediated synaptic signaling is severely disrupted in *Cdk15*^{-y} cortical neurons.**

118 The reduced mGluR5-Homer1bc association that we found suggests that the receptor activity might
119 be compromised (Aloisi et al., 2017; Kammermeier and Worley, 2007). To test this hypothesis, we
120 started by recording spontaneous miniature excitatory postsynaptic currents (mEPSCs) in neuronal
121 cultures of the S1 cortex from both *Cdk15*^{+y} and *Cdk15*^{-y} mice (fig. 2A-D, upper part), before and
122 after mGluR5 activation. As we reported in a previous study (Della Sala et al., 2016), mEPSCs
123 recorded from CDKL5 null neurons showed an increased inter-event interval (IEI) (*Cdk15*^{+y} vs *Cdk15*^{-y}
124 ^y * $p < 0.05$; fig. 2D) while the mean peak amplitude was similar between genotypes (*Cdk15*^{+y} vs
125 *Cdk15*^{-y} $p > 0.05$; fig. 2C). Intriguingly, we found that when cortical neurons were stimulated for two
126 minutes with the selective mGluR5 agonist DHPG (100 μ m), mEPSCs IEI was significantly increased
127 in *Cdk15*^{+y} cultures (fig. 2E, lower part; A) (Moult et al., 2006; Verpelli et al., 2011), but not in *Cdk15*^{-y}
128 ^y neurons (fig. 2E) indicating that CDKL5 loss impacts negatively on mGluR5 signaling in excitatory
129 synaptic transmission. Next, we performed patch-clamp recordings in whole-cell configuration in
130 neuronal cultures from S1 cortex and recorded NMDA currents elicited by NMDA (50 mM) alone
131 (Marcantoni et al., 2020) or together with agonist DHPG (100 μ m) as shown in Reiner et al., 2018
132 (Reiner and Levitz, 2018). Strikingly, *Cdk15*^{-y} cultures showed a significant reduction of I_{NMDA} with
133 respect to *Cdk15*^{+y} neurons (*Cdk15*^{+y}: 869.6 ± 85.4 pA, *Cdk15*^{-y}: 544.2 ± 113.2 pA; ** $p < 0.01$; fig.
134 2F). Next, we found that DHPG increased I_{NMDA} in *Cdk15*^{+y} cells, (fig. 2G; see also Vicidomini et
135 al., 2017) while, interestingly, it was not effective in *Cdk15*^{-y} neurons (fig. 2G), as illustrated by the
136 sharp difference in the percentage of I_{NMDA} change between genotypes (*Cdk15*^{+y}: 38.35%; *Cdk15*^{-y}:
137 -14.47%, $p < 0.05$. Fig. 2G). Strikingly, while 73% of *Cdk15*^{+y} cortical neurons (11/15 cells) showed
138 potentiated I_{NMDA} after the application of DHPG, in most *Cdk15*^{-y} tested neurons we did not observe
139 any effect of DHPG (10/14; 71%). These results disclose novel disrupted mechanisms of excitatory
140 synaptic transmission caused by the absence of CDKL5, selectively involving metabotropic receptors
141 signaling.

142 **2.3 CDPPB potentiates NMDAR current in cortical neurons lacking CDKL5.**

143 We and others have previously shown that in conditions where I_{NMDA} is not sensitive to DHPG,
144 selective mGluR5 PAMs can instead elicit the strengthening of this current (Auerbach et al., 2011;
145 Vicidomini et al., 2017). Among these, 3-Cyano-N-(1,3-diphenyl-1H-pyrazol-5-yl)benzamide
146 (CDPPB) offers several advantages compared to agonist drugs such as higher subtype selectivity,
147 reduced desensitization, and more subtle modulatory effects on receptor function (Chen et al., 2008).
148 We first examined whether CDPPB produces an effect on cortical neurons lacking CDKL5 by
149 measuring NMDA current. Intriguingly, we found that 2 min application of CDPPB (10 μM)
150 preceding NMDA (50 μM) administration produced a comparable increase of I_{NMDA} (Fig. 2F, lower
151 part) in both genotypes ($Cdk15^{+/y}$ 42.92%; $Cdk15^{-/y}$ 45.19%, fig. 2H) if compared to the average
152 amplitude of I_{NMDA} measured after administration of NMDA alone. Interestingly, the majority of both
153 $Cdk15^{-/y}$ and $Cdk15^{+/y}$ neurons showed potentiated I_{NMDA} after the application of CDPPB ($Cdk15^{+/y}$:
154 13/18, 78%; $Cdk15^{-/y}$ 10/12, 83%) resulting in a significantly higher percentage of $Cdk15^{-/y}$ neurons
155 responding to CDPPB compared to DHPG treatment (chi-square $Cdk15^{-/y}$ -DHPG: 29% vs $Cdk15^{-/y}$ -
156 CDPPB: 83% **** $p < 0.0001$). Thus, these results show that positive allosteric modulation can
157 rescue mGluR5-dependent strengthening of NMDA-mediated activation in neurons lacking CDKL5.

158

159 **2.4 CDPPB treatment ameliorates visual, sensorimotor and memory functions in $Cdk15^{-/y}$ mice.**

160 Encouraged by the positive effects that we obtained using CDPPB on synaptic currents, we evaluated
161 the therapeutic potential of this PAM by treating mice with one intraperitoneal injection (i.p.) of
162 CDPPB (3 mg/Kg), as in Vicidomini et al. (2017), and then exposing animals to a battery of tests.

163 We investigated cortical visual responses by transcranial intrinsic optical signal (IOS) imaging before
164 and after CDPPB administration in the same animals. As expected from our previous data (Lupori et
165 al., 2019; Mazziotti et al., 2017), baseline response amplitude of $Cdk15^{-/y}$ mice was strongly decreased
166 compared to $Cdk15^{+/y}$ littermates (one way ANOVA ** $p < 0.01$; Tukey multiple comparison $Cdk15^{+/y}$

167 vs CDPPB-Cdk15^{-y} ** $p < 0.01$; Cdk15^{+y} vs vehicle-Cdk15^{-y} ** $p < 0.01$; vehicle-Cdk15^{-y} vs CDPPB-
168 Cdk15^{-y} $p = 0.92$. Fig. 3A, B). After CDPPB treatment, visual responses approached Cdk15^{+y} levels
169 (one way ANOVA ** $p < 0.01$; Tukey multiple comparison Cdk15^{+y} vs CDPPB-Cdk15^{-y} post
170 injection $p = 0.6$; Cdk15^{+y} vs vehicle-Cdk15^{-y} post injection * $p < 0.05$) significantly increasing from
171 their baseline values (two-way RM ANOVA; main effects not significant, interaction treatment*time
172 * $p < 0.05$; Sidak multiple comparison: vehicle-Cdk15^{-y} post injection vs CDPPB-Cdk15^{-y} post
173 injection * $p < 0.05$; CDPPB-Cdk15^{-y} baseline vs CDPPB-Cdk15^{-y} post injection * $p < 0.05$; vehicle-
174 Cdk15^{-y} baseline vs vehicle-Cdk15^{-y} post injection $p = 0.90$). By contrast, visual response remained
175 impaired in vehicle-treated mutant mice. These experiments indicate that the cortical visual
176 impairment (CVI) shown by Cdk15^{-y} mice can be rescued by CDPPB treatment.

177 When we assessed sensorimotor responses by using the adhesive tape-removal test (Bouet et al.,
178 2009; Komotar et al., 2007), we found that Cdk15^{-y} mice display a significant increase in the time-
179 to-contact the tape compared to Cdk15^{+y} mice (vehicle-Cdk15^{+y} vs vehicle-Cdk15^{-y} ** $p < 0.01$; fig.
180 3C). Importantly, a single CDPPB injection produced a reduction of the latency exclusively in mutant
181 mice whose performance became similar to controls (vehicle-Cdk15^{+y} vs CDPPB-Cdk15^{-y} $p > 0.4$;
182 fig. 3C). Finally, the effect of CDPPB was assessed in the Y-maze paradigm for working memory, a
183 feature known to be impaired in Cdk15^{-y} mutant mice (Fuchs et al., 2014). First, we found that the
184 number of the correct spontaneous alternations is decreased in Cdk15^{-y} mice compared to Cdk15^{+y}
185 animals (vehicle-Cdk15^{+y} vs vehicle-Cdk15^{-y} ** $p < 0.01$; fig. 3D), confirming previous observations.
186 Intriguingly, CDPPB rescued working memory defects in Cdk15^{-y} mice by normalizing the frequency
187 of spontaneous alternations (vehicle-Cdk15^{+y} vs CDPPB-Cdk15^{-y} $p > 0.4$; fig. 3D), without altering
188 the performance of Cdk15^{+y} mice. No difference in the total number of arms entries were found
189 between genotypes under either treated or untreated conditions (fig. 3E). Thus, these data indicate
190 that the action of CDPPB can reverse atypical functional responses, such as CVI and sensorimotor
191 defects, as well as memory impairment shown by Cdk15^{-y} mice.

192 **2.5 mGluR5 PAMs rescue both synaptic and activity defects in *Cdk15*^{-y} cerebral cortex.**

193

194 In parallel with the observed behavioural and functional rescues, we found that the acute CDPPB
195 treatment produced a normalization of the number and organization of postsynaptic sites as well as
196 of the activity in primary cortices of *Cdk15*^{-y} mice. CDPPB increased the density of Homer1bc⁺
197 puncta in both S1 and V1 cortices of *Cdk15*^{-y} mice (S1: layers II-III and layer V vehicle-*Cdk15*^{-y} vs
198 CDPPB-*Cdk15*^{-y} ** $p < 0.01$. V1: layers II-III and layer V vehicle-*Cdk15*^{-y} vs CDPPB-*Cdk15*^{-y} * $p <$
199 0.05; fig. 4A,B), reproducing *Cdk15*^{+y} mice conditions (S1 and V1: layer II-III and layer V: vehicle-
200 *Cdk15*^{+y} vs CDPPB-*Cdk15*^{-y} $p > 0.3$; fig. 4A,B). Intriguingly, CDPPB treatment also normalized
201 mGluR5⁺ puncta density in both S1 and V1 cortices of *Cdk15*^{-y} mice (S1: layers II-III and layer V:
202 vehicle-*Cdk15*^{-y} vs CDPPB-*Cdk15*^{-y} *** $p < 0.001$; vehicle-*Cdk15*^{+y} vs CDPPB-*Cdk15*^{-y} $p > 0.3$. V1:
203 layers II-III and layer V: vehicle-*Cdk15*^{-y} vs CDPPB-*Cdk15*^{-y} * $p < 0.05$. S1 and V1: vehicle-*Cdk15*^{+y}
204 vs CDPPB-*Cdk15*^{-y} $p > 0.3$; fig. 4C,D). Finally, the density of cells expressing ARC, an immediate-
205 early gene induced by mGluR5 activation (Ménard and Quirion, 2012; Wang and Zhuo, 2012), was
206 restored in the V1 cortex of CDKL5-mutants after a single CDPPB administration (layers I-VI:
207 vehicle-*Cdk15*^{+y} vs vehicle-*Cdk15*^{-y} ** $p < 0.01$; vehicle-*Cdk15*^{-y} vs CDPPB *Cdk15*^{-y} *** $p < 0.001$;
208 fig. 4E,F).

209 In order to increase the reproducibility of our study, we treated another group of *Cdk15*^{-y} and *Cdk15*^{+y}
210 animals with a different mGluR5 PAM, the RO6807794 (RO68) compound (Kelly et al., 2018). Two
211 hours after an i.p. injection with RO68 (0.3 mg/kg as in Kelly et al., 2018), we found that the density
212 of Homer1bc⁺ puncta in S1 cortex of *Cdk15*^{-y} mice was increased (S1: layers II-III and layer V
213 vehicle-*Cdk15*^{-y} vs CDPPB-*Cdk15*^{-y} * $p < 0.05$. V1: layers II-III and layer V vehicle-*Cdk15*^{-y} vs
214 CDPPB-*Cdk15*^{-y} * $p < 0.05$; fig. S1 A-B) to reproduce *Cdk15*^{+y} mice conditions (S1 layer II-III and
215 layer V: vehicle-*Cdk15*^{+y} vs CDPPB-*Cdk15*^{-y} $p > 0.3$; fig. S1 A-B). Intriguingly, RO68 was also able
216 to restore neuronal activity in S1 cortex in *Cdk15*^{-y} mice (Fig. S1 C) throughout cortical layers
217 (vehicle-*Cdk15*^{+y} vs vehicle-*Cdk15*^{-y} *** $p < 0.001$; vehicle-*Cdk15*^{-y} vs RO68-*Cdk15*^{-y} *** $p <$

218 0.001), as indicated by the c-Fos⁺ cell density count (Fig. S1 D; see also Pizzo et al., 2016), that
219 reached the magnitude of Cdk15^{+/-} mice (vehicle Cdk15^{+/-} vs CDPPB-Cdk15^{-/-} p > 0.05). These results
220 strongly support the idea that the atypical organization, both structural and molecular, of the neural
221 circuits in the cerebral cortex of Cdk15^{-/-} mutants can be rescued by activating mGluR5-mediated
222 signaling.

223

224 ***2.6 The effects of a protracted CDPPB treatment in Cdk15^{-/-} mice are long-lasting.***

225 To assess the therapeutic potential of mGluR5 activation, we treated animals for five consecutive
226 days with CDPPB and 24 hours after the last injection animals were behaviourally tested and then
227 sacrificed for brain analyses. We found that, after this protracted treatment, the density of Homer1bc⁺
228 puncta remained increased in both upper and deeper layers of the S1 cortex in mutant mice (layers II-
229 III and layer V: vehicle-Cdk15^{-/-} vs CDPPB-Cdk15^{-/-} p < 0.01; fig. 5A, B), and that its value was no
230 longer different from control (layers II-III and layer V: vehicle-Cdk15^{+/-} vs CDPPB-Cdk15^{-/-} p > 0.3;
231 fig. 6B). In contrast, no effect of CDPPB on Homer1bc expression was found in Cdk15^{+/-} animals
232 (layers II-III and layer V: vehicle-Cdk15^{+/-} vs CDPPB-Cdk15^{+/-} p > 0.9; fig. 5A, B). Next, we analysed
233 hind-limb clasping, a sign displayed shown by Cdk15^{-/-} mice (Amendola et al., 2014; Terzic et al.,
234 2021; Trazzi et al., 2018). In line with previous studies, vehicle-treated mutants showed increased
235 hind-limb clasping compared to Cdk15^{+/-} littermates (vehicle-Cdk15^{+/-} vs vehicle-Cdk15^{-/-} p < 0.001;
236 fig. 5C -Amendola et al., 2014) whereas after CDPPB treatment Cdk15^{-/-} mice spent significantly less
237 time clasping their hind paws (vehicle-Cdk15^{-/-} vs CDPPB-Cdk15^{-/-} p < 0.01; fig. 5C), although
238 CDPPB did not produce a complete normalization (vehicle-Cdk15^{+/-} vs. CDPPB-Cdk15^{-/-} p < 0.01;
239 fig. 5C). Finally, we evaluated the effects of sub-chronic CDPPB treatment on cortical activity by
240 analysing c-Fos expression. The effect of CDPPB treatment was subtle (vehicle-Cdk15^{+/-} vs vehicle-
241 Cdk15^{-/-} p < 0.01; vehicle-Cdk15^{-/-} vs CDPPB-Cdk15^{-/-} p = 0.09; fig. 5 D,E) but sufficient to normalize
242 c-Fos levels in mutant mice (vehicle Cdk15^{+/-} vs CDPPB-Cdk15^{-/-} p > 0.09; fig. 5E). Taken together,

243 these data indicate that protracted CDPPB treatment is accompanied by long-lasting positive effects
244 in *Cdk15^{-y}* mice, a result consistent with the design of a therapeutic protocol for CDD targeting
245 mGluR5.

246

247 ***2.7 The BA17 cortex of CDD patients recapitulates the mGluR5 defects shown by *Cdk15^{-y}* mice.***

248 Finally, to assess the translational potential of our findings, we examined excitatory synaptic
249 structures in the 2 postmortem CDD patient brains available worldwide that we obtained from the
250 Harvard Brain Tissue Resource Center (Belmont; USA). These experiments were performed on
251 sections from the primary visual cortex (BA17) of CDD cases and age/sex-matched neurotypical
252 subjects (NTs). Intriguingly, the results showed a clear reduction of both postsynaptic proteins PSD-
253 95⁺ and Homer1bc⁺ as well as of the presynaptic marker VGluT1⁺, irrespective of case age (5 and 30
254 years old), compared to NTs (fig. 6A)). Moreover, although a statistical analysis was not performed
255 with only 2 cases, the quantification of the immunopuncta revealed a reduction in the cortices of CDD
256 patients compared to NTs (fig. 6A-D), indicative of an overall reduction of glutamatergic synapses.
257 We next evaluated Homer1bc, PSD-95 and mGluR5 expression by western blotting on BA17 cortex
258 lysates. Intriguingly, as shown in figures 6 E-H, the BA17 area from CDD samples showed a robust
259 reduction of their expression compared to NTs. Although derived from a limited dataset, these results
260 suggest for the first time that both structural and molecular signatures of CDKL5 loss largely overlap
261 between mice and human cortical connectivity and support the translational potential of a mGluR5-
262 directed therapeutic strategy.

263

264 3. Discussion

265 It is urgent to find therapeutic targets that shall be rapidly translated into treatments for CDD, a
266 devastating condition without corrective options. In this study, we focus our attention on mGluR5, a
267 group I metabotropic glutamate receptor highly expressed in the cerebral cortex of both mice and
268 humans (Ferraguti & Shigemoto, 2006). To properly function, mGluR5 requires binding with
269 Homer1bc (Aloisi et al., 2017), a scaffolding protein that is severely downregulated in the cerebral
270 cortex of both CDKL5^{-y} mice and CDD patients (Pizzo et al., 2019, 2016; fig. 6A) as well as in
271 iPSCs-derived neurons from CDD patients (Negraes et al., 2021).

272 We here show for the first time that CDKL5 plays a role in the expression of mGluR5 in the cerebral
273 cortex of both CDD patients and CDKL5 mutant mice, an effect likely produced by the defective
274 formation of mGluR5-Homer1bc complexes at synapses as indicated by our data. Moreover, we find
275 that synaptic transmission, both basal and NMDA-mediated, is altered in S1 neurons lacking CDKL5
276 and that it is unresponsive to the modulation normally produced by the selective mGluR5 agonist
277 DHPG. Because Shank1, by forming complexes with Homer1bc, PSD-95 and NMDAR, promotes
278 the cooperation between NMDAR and mGluR5 signaling machineries (Ango et al., 2000; Hering and
279 Sheng, 2001; Tu et al., 1999), our electrophysiological evidences strongly suggest that lack of
280 CDKL5 tampers with the synergistic cooperation between these glutamatergic receptors. This effect
281 is likely produced by a reduced amount of Homer1bc recruited in the postsynaptic density in the
282 absence of CDKL5 which, in turn, results in an atypical postsynaptic localization/stabilization of
283 mGluR5. Interestingly, aberrant NMDA receptors signaling have been previously reported by Okuda
284 and colleagues (2017) in the hippocampus of a different CDKL5 mutant mice line showing severe
285 NMDA-dependent epileptic seizures due to the incorrect postsynaptic accumulation of GluN2B-
286 containing NMDA receptors (Okuda et al., 2017). Similar results have been obtained in the
287 hippocampus of the Cdk15^{R59X} knock-in CDD mouse model (Yennawar et al., 2019). Altogether,
288 although with some differences, these findings further support the idea that CDKL5 plays a crucial

289 role in the correct localization/function of glutamate receptors, both ionotropic and metabotropic, at
290 the synapse. Remarkably, an aberrant expression and function of mGluR5 has been reported in several
291 neurodevelopmental diseases such as Fragile X, Phelan McDermid syndrome, Tuberous sclerosis
292 (TSC) and Rett syndrome (Aloisi et al., 2017; Auerbach et al., 2011; Gogliotti et al., 2016; Vicidomini
293 et al., 2017) further supporting the primary role of mGluR5 signaling as common deranged pathway
294 in monogenetic forms of neurodevelopmental disorders.

295 The reduced expression/function of mGluR5, combined with relevant synaptic and behavioural signs
296 shown by CDKL5 mutant mice, provided us with solid bases for attempting the first preclinical
297 assessment of mGluR5 PAMs efficiency for treating CDD that we report in this study. Intriguingly,
298 our results revealed that an acute treatment with CDPPB is effective in restoring several
299 endophenotypes and behavioural signs produced by CDKL5 loss both *in-vitro* and *in-vivo*. Our data
300 show that in primary cortical neuronal cultures, CDPPB can restore mGluR5-mediated potentiation
301 of NMDA currents in *Cdkl5^{-y}* pyramidal neurons. Considering the negative response of NMDA
302 current to DHPG treatment that we report in mutant neurons, the effect of CDPPB is surprising and
303 still without a clear pharmacological explanation, although it closely replicates what has been found
304 previously in Shank3-KO neurons (Vicidomini et al., 2017). Furthermore, the present findings
305 strongly suggest that CDPPB treatment can facilitate the functional maturation of dendritic spines in
306 the absence of CDKL5, as it increases the synaptic expression of both Homer1bc and mGluR5, two
307 crucial molecular determinants of spine formation and stabilization (Oh et al., 2013; Sala et al., 2003).
308 These synaptic effects are reflected by beneficial outcomes at the functional and behavioural level in
309 mutant animals that are mostly relevant in the context of CDD. Our data, showing for the first time
310 that both CVI and overall cortical activity can be rescued by CDPPB treatment in *Cdkl5^{-y}* mice,
311 strengthens the translational value of our preclinical results. As a matter of fact, recent data indicate
312 that CVI is correlated with reduced milestone achievement in CDD patients and therefore CVI can

313 be used in the clinic as a solid biomarker for CDD diagnosis, progression, and treatment with
314 biunivocal translational validity(Demarest et al., 2019; Mazziotti et al., 2017).

315 Interestingly, our findings indicate that mGluR5 signaling greatly suffers from the lack of CDKL5,
316 but it does not become completely non-functional. In support of this idea, our data show that the
317 protracted treatment with CDPPB in CDKL5-null mice produces long-lasting rescuing effect on both
318 the density of dendritic spine-like structures and cortical c-Fos expression in the cerebral cortex as
319 well as on the hindlimb-clasping phenotype. Thus, although further studies are needed to dissect out
320 the mechanisms of CDPPB action on excitatory synapse signaling, our results encourage further
321 testing of mGluR5 PAMs in animals modelling CDD and offer hope for a future use of these
322 compounds in the clinic. Our set of data obtained with another mGluR5 PAM, the RO68 compound,
323 further strengthen this idea. Considerably, RO68 has the clinically relevant advantage that it can be
324 dissolved in salina with an extremely low percentage of detergent (i.e.: Tween-80) and has a higher
325 potency compared to other mGluR5 PAMs. Remarkably, RO68 is efficacious even at very low
326 concentrations (i.e.: 0.3 mg/kg), thus reducing the risk of toxicity, as we show in this study where this
327 compound was able to rescue neuroanatomical, functional and behavioural signs of CDKL5 mutant
328 mice, and as it was previously shown in a mouse model of TSC (Kelly et al., 2018).

329 Finally, the positive action of mGluR5 PAMs on the molecular organization of postsynaptic structures
330 is encouraging in view of the data we have obtained from the only two post-mortem CDD brains
331 available. Remarkably, we show, for the first time, that the lack of CDKL5 induces the
332 disorganization of the excitatory synaptic compartment in the BA17 cortical area of CDD human
333 brains both the localization and expression of several synaptic molecules (i.e. VGluT1, Homer1bc,
334 PSD-95 and mGluR5) seems negatively affected, as we and others previously reported in CDKL5-
335 null mice (Pizzo et al., 2019, 2016; Trazzi et al 2018; Amendola et al., 2016). These results, when
336 confirmed on a larger group CDD brains, shall contribute to disclose the connectivity impairments of
337 the primary visual cortex underlying CVI in these patients (Demarest et al., 2019) and strengthen the

338 face-validity of CDKL5^{-y} mice in closely modelling the neuropathological signs of CDD.
339 Importantly, our data indicate that the synaptic abnormalities and mGluR5 downregulation occurring
340 in human CDD patients are potentially rescuable by positive allosteric modulation of mGluR5.

341 In further support of our findings, Negraes et al. have found similar synaptic defects in iPSCs-derived
342 cortical neurons from CDD patients (Negraes et al., 2021). In apparent contrast from our observation,
343 they found an increased mGluR5-PanHomer association in CDD human organoids (Negraes et al.,
344 2021) while we revealed that mGluR5-Homer1bc binding, an association crucial for this receptor
345 function, is decreased in CDKL5 mutant mice. The most parsimonious explanation of this
346 discrepancy arises primarily either the different technical approaches or the experimental models used
347 (i.e., mice brain vs CDD human organoids). Moreover, in Negraes et al. no discrimination between
348 different Homer isoforms has been attempted, although it is known that the binding between mGluR5
349 and Homer1bc or Homer1a produces opposite effects on mGluR5 membrane expression and function
350 (Menard and Quirion, 2012; Shiraishi-Yamaguchi and Furuichi, 2007; Bertaso et al., 2010). Hence,
351 the enhanced mGluR5-Pan-Homer interaction could be produced by an increased association with
352 Homer1a, thus not ruling out a decreased mGluR5-Homer1bc binding as revealed by our study.

353 In conclusion, we believe that our findings on the efficacy of mGluR5 activation pave the way for
354 including these receptors as a promising therapeutic target for CDD. Our results also suggest that an
355 early-onset and prolonged regime of mGluR5 activation has the potential to stably revert the
356 morphofunctional defects shown by adult CDKL5 mutants. Finally, this study further supports
357 previous indications that abnormalities of mGluR5 signaling represents a convergent pathway for
358 multiple neurodevelopmental diseases, a solid hallmark now including CDD.

359

360 **4. Materials and Methods**

361 **Animals and pharmacological treatment**

362 Animal care and handling throughout the experimental procedures were conducted in accordance
363 with European Community Council Directive 2010/63/UE for care and use of experimental animals
364 with protocols approved by the Italian Minister for Scientific Research (Authorization number
365 38/2020-PR) and the Bioethics Committee of the University of Torino, Italy. Animal suffering was
366 minimized, as was the number of animals used. Mice for testing were produced by crossing $Cdk15^{-/x}$
367 females with $Cdk15^{-/y}$ males or with $Cdk15^{+/y}$ males. Littermate controls were used for all the
368 experiments. After weaning, mice were housed 4 per cage on a 12 h light/dark cycle (lights on at 7:00
369 h) in a temperature-controlled environment ($21 \pm 2^\circ\text{C}$) with food and water provided ad libitum. For
370 this study, 8-weeks old (post-natal day 56) $Cdk15^{-/y}$ and $Cdk15^{+/y}$ males were used. Because we did
371 not observe any noticeable interindividual phenotypic or metabolic (e.g. weight and health condition
372 scores) difference among the mouse cohorts used in this study, no inclusion/exclusion criteria were
373 adopted besides age (PND56) and sex (male) of the animals. In pharmacological rescue experiments,
374 animals were treated with the selective positive allosteric modulator (PAM) of mGluR5 3-cyano-N-
375 (1,3-diphenyl-1H-pyrazol-5-yl)benzamide (CDPPB; Tocris, UK) that was diluted in saline solution
376 containing 5-10% final concentration of DMSO and polyethylene glycol 400 (DMSO: PEG 400 =
377 1:9) 5,23. Acutely treated mice received an intraperitoneal injection (ip) of either CDPPB (3 mg/kg)
378 or vehicle 5 at 9.00 am and then put back in their home cage for 1 hour before being behaviourally
379 tested. For sub-chronic administration, animals were treated for five consecutive days and, 24 hours
380 after the last injection, tested and after one hour from the behavioural test, the animals were sacrificed.
381 All mice were subsequently sacrificed for brain analyses. All analyses presented in this study were
382 carried out by investigators who were blinded to the animal's/neuronal genotype or treatments.

383

384 **Synaptosomal fraction preparation**

385 Adult mice (PND 56) were killed by decapitation, the entire cortex was rapidly removed and tissue
386 was processed as in 61,62. The tissues were homogenized in ice-cold lysis buffer (0.32 M sucrose,
387 and HEPES 1X at pH 7.4 and 1 mM EGTA, 1mM Na-Orthovanadate, 1 mM DTT,
388 phenylmethylsulphonyl fluoride and 1 mM sodium fluoride and protease inhibitors (SIGMAFAST™
389 Protease Inhibitor Cocktail Tablets, EDTA-Free), using a glass Teflon tissue grinder. The
390 homogenates were centrifuged at 1000 g for 10 min at 4°C. After discarding the nuclear pellet, the
391 supernatant was centrifuged at 12,500 g for 20 min at 4°C. The P1 fraction was then washed with the
392 same initial volume of lysis buffer and underwent further spin (20 min; 12,500 g). The pellet obtained
393 was the crude cortical synaptosomal fraction (P2) that was resuspended in 400 µl of RIPA buffer (NP-
394 40 1%, Na deoxycholate 0,25%, EDTA 0.5M, NaCl 5M, Tris pH8 1M, SDS 10%) and stored at -
395 80°C. Protein concentration of the synaptosomal fraction was determined with the Bio-Rad protein
396 assay kit.

397 **Co-immunoprecipitation assay**

398 50 µg of proteins from the crude synaptosomal (P2) fractions were incubated for 1 hour at 4 °C in
399 RIA buffer (200 mM NaCl, 10 mM EDTA, 10 mM Na₂HPO₄, 0.5% Nonidet P-40 supplemented
400 with 0.1% SDS) and protein A/G-agarose beads (Santa Cruz, Dallas, TX, USA) as pre-cleaning
401 procedure. The beads were then let to sediment at the bottom of the tube and the supernatant was
402 collected. Primary antibody (Homer1bc) was added to the supernatant before leaving to incubate
403 overnight (O/N) at 4 °C on a rotating wheel, then protein A/G-agarose beads were added and
404 incubation continued for 2h at RT. Beads were then collected by gravity and washed three times with
405 RIA buffer before adding sample buffer for SDS–polyacrylamide gel electrophoresis (SDS–PAGE)
406 and heating the mix at 95°C for 10 min. Beads were pelleted by centrifugation and supernatants were
407 separated using 4–15% SDS–PAGE precast gels (Biorad, Italy) (Mellone et al., 2015).

408 **Human postmortem brain tissue**

409 The CDKL5 specimens were provided by the Harvard Brain Tissue Resource Center, Belmont
410 (USA). Case P1 was a 5.7-year-old female with a frameshift mutation (c.2153_2154dupTG) in exon
411 15 of CDKL5 gene that results in a premature stop codon. Case P2 was a 30-year-old female with a
412 deletion of exons 1-3 in CDKL5 gene. Control samples were obtained from the University of
413 Maryland, Baltimore. Case C1 was a 4 years old female whereas case C2 was a 29 years old female.
414 The sections analysed are from the BA17 occipital region of human cerebral cortex. Some sections
415 were lysate for western blot analyses, others for immunofluorescences. While, six 30 µm-thick
416 sections were pull down for each samples, and processed with RIPA buffer (NP-40 1%, Na
417 deoxycholate 0,25%, EDTA 0.5M, NaCl 5M, Tris pH8 1M, SDS 10%).

418 **Western blotting**

419 Lysates both immunoprecipitates and the inputs (50% of the total P2 lysates) and from human brains
420 were boiled in SDS sample buffer, separated by SDS-PAGE and the proteins were then blotted to
421 PVDF membrane following a standard protocol (Grasso et al., 2017). Next, PVDF membranes were
422 blocked in BSA 5% for 1h and incubated with the primary antibodies (see table 2) O/N at 4°C. After
423 washes with TBS 0.1% Tween 20, the membranes were incubated with the appropriate secondary
424 antibodies (anti-mouse or anti-rabbit, 1:5000; Sigma, Italy) for 1h at RT. The chemiluminescent
425 signal was visualized using Clarity™ Western ECL Blotting Substrates (Bio-Rad; Italy) and acquired
426 with Bio-Rad ChemiDoc™ Imagers (Bio-Rad; Italy) and analysed with Image J software (NIH,
427 Usa).

428 **Immunofluorescence procedures**

429 Cerebral cortical tissue: for synaptic proteins detection, mice were anesthetized using a mix of
430 tiletamine/zolazepam (40mg/kg) and xilazine (4-5 mg/kg) and then decapitated 20. The brains were

431 rapidly excised and manually cut in coronal slabs that were fixed by immersion in ice-cold
432 paraformaldehyde (4% in 0.1M phosphate buffer, PB, pH 7.4) for 30 min. After fixation, tissue slabs
433 were rinsed in PB 0.1M, cryoprotected by immersion in sucrose-PB 0.1M solutions (10, 20 and 30%),
434 cut in 20- μ m sections with a cryostat, mounted on gelatine-coated slides and stored at -20°C until
435 immunolabeling was performed as in 20. For c-Fos, ARC and Homer1bc immunodetection after
436 CDPPB subchronic treatment, animals were anesthetized tiletamine/zolazepam (40mg/kg) and
437 xilazine (4-5 mg/kg) and transcardially perfused with about 10 ml of 0.1M PBS followed by 80 ml
438 of ice-cold 4% paraformaldehyde in 0.1M PB. After the brains were dissected, they were kept in the
439 same fixative solution O/N at 4°C , cryoprotected by immersion in raising sucrose-PB 0.1M solutions
440 (10, 20 and 30%), cut into 30 μ m sections with a cryostat and stored at -20°C in a cryoprotectant
441 solution containing 30% ethylene glycol and 25% glycerol until use. Cryosections were subsequently
442 processed free-floating by immersion in 0.1M PBS solution containing 3% normal donkey serum
443 (NDS) and 0.5% Triton X for 1h followed by an O/N incubation at 4°C with the primary antibodies
444 (see table 2). The following day the sections were rinsed with 0.1M PBS and incubated with the
445 appropriate fluorescent secondary antibodies (anti-mouse or anti-rabbit 1:1000; Jackson
446 ImmunoResearch, West Grove, PA, USA) for 1h at RT. The sections were washed three times with
447 PBS, mounted on gelatine-coated glass slides and cover slipped with Dako fluorescence mounting
448 medium (Dako Italia, Italy).

449 Human postmortem brain tissue: immunofluorescence was performed on flash-frozen sections. Serial
450 sections (20 μ m) were cut by using a cryostat, mounted on superfrost slides and stored at -80°C until
451 immunolabeling was performed. Before starting the immunofluorescence, sections were fixed in cold
452 methanol for 1 min. The sections were then processed for double immunofluorescence by using in
453 combination anti-Homer1bc and anti-PSD-95 primary antibodies and the appropriate fluorescent
454 secondary antibodies (anti-mouse or anti-rabbit 1:1000; Jackson ImmunoResearch, West Grove, PA,
455 USA) following the same protocol used for mouse brain tissue (see Pizzo et al., 2016).

456 **Images acquisition and analysis**

457 For brain sections analyses, the layers of the mouse primary somatosensory and visual (S1 and V1)
458 cortices were identified as previously reported (Tomassy et al., 2014; van Brussel et al., 2009).
459 Synaptic immunofluorescence puncta, for both mouse and human brain tissue, were analysed on 5
460 serial optical sections (0.5 μm Z-step size) acquired from layers 2-3 and 5 of S1 and V1 with a laser
461 scanning confocal microscope (LSM5 Pascal; Zeiss, DE) using a 100 \times oil objective (1.4 numerical
462 aperture) and the pinhole set at 1 Airy unit. The density of the immunopositive puncta was determined
463 by manual count followed by density analysis (puncta/100 μm^2) with Imaris (Bitplane, Zurich, CH)
464 and Image J (USA) softwares. Synaptic puncta were included if present in at least two consecutive
465 optical sections.

466 For ARC and c-Fos immunofluorescence analyses, confocal images of the mouse S1 and V1 cortices
467 were acquired in at least three corresponding coronal brain sections from at least six animals per
468 group with a 20 \times objective using a 1- μm Z-step. Digital boxes spanning from the pial surface to the
469 corpus callosum were superimposed at matched locations on each coronal section of V1 and divided
470 into 10 equally sized sampling areas (bins; layer I: bin 1; layer II/III: bins 2–3; layer IV: bins 4–5;
471 layer V: bins 6–7; layer VI: bins 8–10) as in (Tomassy et al., 2014). The density of ARC⁺ cells was
472 determined by manual count in each bin using Image J software and expressed as cells/mm², while
473 intensity values of c-Fos⁺ cells were obtained using a dedicated Image J tool (integrative density) to
474 analyse Z-stack projected images (Sum value).

475 **Chronic IOS Imaging**

476 Surgery: for chronic IOS preparations, adult mice were anesthetized and maintained with isoflurane
477 (respectively 3 and 1%), placed on a stereotaxic frame and head fixed using ear bars. Body
478 temperature was controlled using a heating pad and a rectal probe to maintain the animals' body at
479 37°C. Local anaesthesia was provided using subcutaneous lidocaine (2%) injection and eyes were

480 protected with dexamethasone-based ointment (Tobradex, Alcon Novartis). The scalp was removed,
481 and the skull carefully cleaned with saline. Skin was secured to the skull using cyanoacrylate. Then
482 a thin layer of cyanoacrylate is poured over the exposed skull to attach a custom-made metal ring (9
483 mm internal diameter) centred over the binocular visual cortex. When the glue dried off, a drop of
484 transparent nail polish was spread over the area to ameliorate optical access. After surgery the animals
485 were placed in a heated box and monitored to ensure the absence of any sign of discomfort. Before
486 any other experimental procedure, mice were left to recover for 24/48h. During this period,
487 paracetamol (5 mg/ml) was administered in the water as antalgic therapy.

488 Visual stimulation, data acquisition and analysis: IOS recordings were performed under Isoflurane
489 (1%) and Chlorprothixene (1.25mg/Kg, i.p.). Images were visualized using an Olympus microscope
490 (BX50WI). Red light illumination was provided by 8 red LEDs (625 nm, Knight Lites KSB1385-1P)
491 attached to the objective (Zeiss Plan-NEOFLUAR 5x, NA: 0.16) using a custom-made metal LED
492 holder. The animal was secured under the objective using a ring-shaped neodymium magnet
493 (www.supermagnete.it, R-12-09-1.5-N) mounted on an arduino-based 3D printed imaging chamber
494 that also controls eye shutters and a thermostated heating pad. Visual stimuli were generated using
495 Matlab Psychtoolbox and presented on a gamma corrected 9.7-inch monitor, placed 10 cm away from
496 the eyes of the mouse. Sine wave gratings were presented in the binocular portion of the visual field
497 (-10° to $+10^{\circ}$ relative to the horizontal midline and -5° to $+50^{\circ}$ relative to the vertical midline) with a
498 spatial frequency of 0.03 cycles per degree, mean luminance 20 cd/m² and a contrast of 90%. The
499 stimulus consisted in the abrupt contrast reversal of a grating with a temporal frequency of 4 Hz for
500 1 sec, time locked with a 16-bit depth acquisition camera (Hamamatsu digital camera C11440) using
501 a parallel port trigger. Interstimulus time was 14 sec. Frames were acquired at 30 fps, with a resolution
502 of 512 x 512 pixels. A total of 270 frames were captured for each trial: 30 before the stimulus as a
503 baseline condition and 240 as post-stimulus. The signal was averaged for at least 30 trials and
504 downsampled to 10 fps. Fluctuations of reflectance (R) for each pixel were computed as the

505 normalized difference from the average baseline ($\Delta R/R$). For each recording, an image representing
506 the mean evoked response was computed by averaging frames between 0.5 to 2.5 sec after
507 stimulation. The mean image was then low-pass filtered with a 2D average spatial filter (30 pixels,
508 $117 \mu\text{m}^2$ square kernel). To select the binocular portion of the primary visual cortex for further
509 analysis, a region of interest (ROI) was automatically calculated on the mean image of the response
510 by selecting the pixels in the lowest 30% $\Delta R/R$ of the range between the maximal and minimal
511 intensity pixel 26. To weaken background fluctuations a manually selected polygonal region of
512 reference (ROR) was subtracted. The ROR was placed where no clear response, blood vessel artifact
513 or irregularities of the skull were observed 27. Mean evoked responses were quantitatively estimated
514 as the average intensity inside the ROI.

515 **Electrophysiology**

516 Primary neuronal cultures: experiments were performed on cortical neurons obtained from 18-day
517 old embryos of both Cdk15^{+/y} and Cdk15^{-y} mice. The S1 cortex was rapidly dissected under sterile
518 conditions, kept in cold HBSS (4°C) with high glucose, and then digested with papain (0,5 mg/ml)
519 dissolved in HBSS plus DNase (0,1 mg/ml). Isolated cells were then plated at the final density of
520 1200 cells/mm². The cells were incubated with 1% penicillin/streptomycin, 1% glutamax, 2.5% fetal
521 bovine serum, 2% B-27 supplemented neurobasal medium in a humidified 5% CO₂ atmosphere at
522 37°C. Experiments were performed at DIV 16 - 18.

523 Patch-clamp recordings: experiments were performed in voltage clamp conditions and whole-cell
524 configuration as in Marcantoni et al., 2010. Patch electrodes, fabricated from thick borosilicate
525 glasses (Hilgenberg, Mansfield, Germany), were pulled to a final resistance of 3-5 M Ω . Patch Clamp
526 recordings were performed in whole cell configuration using a Multiclamp 700-B amplifier connected
527 to a Digidata 1440 and governed by the pClamp10 software (Axon Instruments, Molecular Devices
528 Ltd, USA). NMDAR activated currents were recorded by holding neurons at -70 mV and perfusing

529 them with the NMDAR agonist, N-Methyl-D-aspartate, (NMDA, 50 μ M). The external solution
530 contained (in mM): 130 NaCl, 1.8 CaCl₂, 10 HEPES, 10 glucose, 1.2 Glycine (pH 7.4). The internal
531 solution contained (in mM): 90 CsCl, 20 TEACl, 10 glucose, 1 MgCl, 4 ATP, 0.5 GTP, 15
532 phosphocreatine (pH 7.4). These experiments were performed in the presence of the AMPA and
533 GABA_A receptors blockers 6,7-dinitroquinoxaline-2,3-dione, DNQX (20 μ M, Sigma-Aldrich) and
534 picrotoxin (100 μ M), respectively. Tetrodotoxin (TTX 0.3 μ M) was added to block voltage-gated
535 Na⁺ channels. The mGluR5 were selectively activated for 2 min either by the agonist DHPG (100
536 μ M) or the positive allosteric modulator CDPPB (10 μ M).

537 Miniature post-synaptic currents (mPSCs): were recorded by holding neurons at -70 mV, recording
538 for 120 seconds, and superfusing the postsynaptic neuron with a Tyrode's solution containing (in
539 mM): 2 CaCl₂, 130 NaCl, 2 MgCl₂, 10 HEPES, 4 KCl, and 10 glucose, pH 7.4. The standard internal
540 solution was (in mM): 90 CsCl, 20 TEA-Cl, 10 EGTA, 10 glucose, 1 MgCl₂, 4 ATP, 0.5 GTP, and
541 15 phosphocreatine, pH 7.4. Picrotoxin is added to the Tyrode solution to block GABA A-dependent
542 currents. Tetrodotoxin (TTX, 0.3 μ M) will be added for the measure of miniature postsynaptic
543 currents in order to block spontaneous action potentials propagation. Cells were then treated for 2
544 minutes with DHPG (100 μ M). Analysis of peak amplitudes and inter-event intervals (IEI) was
545 performed with Clampfit software (Axon Instruments).

546 **Behavioural analyses**

547 For the acute treatment regime, 1h after a single i.p. injection with either CDPPB or vehicle, animals
548 were probed with adhesive tape removal test and Y-maze test. For the subchronically treated mice,
549 24h after the last injection hind-limb clasping behaviour was tested.

550 Adhesive tape removal test: sensorimotor abilities were evaluated using the adhesive tape removal
551 test as previously described. Briefly, P56 mice were habituated to the testing room for 30 min before
552 starting the experiment and then single animals were placed in the testing cage for the habituation

553 period of 60 sec. The animal was then removed from the testing box and an adhesive tape strip (0.3
554 cm x 0.4 cm) was placed on the bottom of one forepaw while the other one was lightly touched by
555 the operator with the same pressure. Animals were put back in the testing cage and the latency to
556 touch the tape was recorded with a cut off time of 2 min.

557 Y-maze test: spontaneous alternation test was used to evaluate spatial working memory in mice. We
558 used an in-house fabricated Y maze that is composed of three arms (34 cm × 5 cm × 10 cm) angled
559 at 120° from one another and made by gray opaque plastic material. Each mouse was placed at the
560 centre of the maze where it can freely explore the three arms for 8 min. Arm entries were defined by
561 the presence of all four paws in an arm. The percentage of spontaneous alternations was calculated
562 as follows: $(\text{total alternations} / \text{total arm entries} - 2) \times 100$.

563 Hind-limb clasping: the presence of hind-limb clasping behaviour was tested by suspending the mice
564 from their tail for 2 min and video recorded. Hind-limb clasping scores were assessed as in (Amendola
565 et al., 2014).

566 **Statistical analysis**

567 All data are reported as mean ± SEM. For the animal experiments, n = number of mice. All statistical
568 analyses were performed using Prism software (Graphpad, La Jolla, CA, USA). For co-IP
569 experiments, one-way analysis of variance (ANOVA) followed by Fisher's post hoc test was used.
570 For the behavioural and anatomical analyses, Student's t-test or two-way ANOVA followed by
571 Fisher's LSD post hoc test were performed, as indicated in the text. For electrophysiology analyses,
572 Student's t-test and chi-square were used, as indicated in the text. All the raw data are reported in
573 table S1. The statistical analysis performed and the n for each experimental group are reported in
574 figure legends.

575
576
577

578 Table1. Mean \pm SEM values for each statistical analysis

Figure 1			Cdk15^{+y}		Cdk15^{-y}		
B	mGluR5/Homer1bc (O.D)		0.254 \pm 0.062		0.174 \pm 0.026		
D	mGluR5 ⁺ puncta /100 μ m ²	LII-III	68.28 \pm 6.23		51.20 \pm 1.68		
		L V	59.63 \pm 3.19		46.01 \pm 2.75		
Figure 2			Cdk15^{+y}		Cdk15^{-y}		
C	Peak amplitude (pA)		21.71 \pm 1.51		21.95 \pm 1.56		
D	Inter-event interval (IEI)		200.8 \pm 33.62		333.6 \pm 54.95		
E	%IEI	Control	100 \pm 16.75		100 \pm 16.47		
		DHPG	329.3 \pm 54.43		162.2 \pm 34.90		
F	NMDA current		869.60 \pm 84.22		433.98 \pm 88.09		
G	Variation (%)	DHPG	38.35 \pm 16.96		-14.47 \pm 13.32		
H	Variation (%)	CDPPB	42.92 \pm 10.27		45.19 \pm 14.75		
Figure 3			Vehicle		CDPPB		
B	Amplitude (Δ R/R)	Baseline	-7.14 \pm 1.21	-3.54 \pm 0.32		-3.8 \pm 0.53	
		Post-injection		-3.29 \pm 0.67		-5.77 \pm 0.86	
C	Time to contact (Sec)		31.33 \pm 6.03	59.38 \pm 6.39	42.70 \pm 6.61	39.88 \pm 8.88	
D	Alternation (%)		67.03 \pm 3.36	46.26 \pm 3.63	64.21 \pm 3.41	60.97 \pm 3.19	
E	Nr entrance		19.43 \pm 1.87	18.29 \pm 4.20	16.28 \pm 2.33	22.43 \pm 1.41	
Figure 4			Vehicle		CDPPB		
B	Homer1bc ⁺ puncta/100 μ m ²	S1	LII-III	82.13 \pm 4.94	61.22 \pm 4.23	83.40 \pm 6.81	77.93 \pm 7.61
			L V	77.15 \pm 2.82	59.40 \pm 4.41	76.22 \pm 7.42	72.08 \pm 5.77
		V1	LII-III	92.80 \pm 7.00	68.88 \pm 1.81	103.1 \pm 4.46	95.95 \pm 6.21
			L V	96.00 \pm 3.38	67.23 \pm 3.03	90.38 \pm 10.27	87.75 \pm 6.81
D	mGluR5 ⁺ puncta /100 μ m ²	S1	LII-III	83.72 \pm 1.28	61.06 \pm 2.86	88.37 \pm 2.33	83.07 \pm 5.56
			L V	80.00 \pm 6.38	51.90 \pm 1.91	81.63 \pm 2.88	81.97 \pm 1.97
		V1	LII-III	95.38 \pm 4.74	65.87 \pm 6.14	78.8 \pm 9.70	93.72 \pm 3.93
			L V	88.05 \pm 4.64	57.14 \pm 5.28	80.82 \pm 9.99	78.63 \pm 7.93
F	ARC ⁺ cells /mm ²	L I	0 \pm 0	0 \pm 0	0 \pm 0	0 \pm 0	
		L II-III	103.5 \pm 20.75	41.19 \pm 14.8	131.5 \pm 63.43	127.3 \pm 5.38	
		L IV	365.9 \pm 74.42	81.62 \pm 18.1	251.6 \pm 179.3	296.5 \pm 133.9	
		L V	255.8 \pm 40.13	91.2 \pm 19.97	389.4 \pm 221.6	367.7 \pm 20.3	
		L VI	672.1 \pm 83.87	470.9 \pm 60.2	998.0 \pm 90.15	1031 \pm 140.5	
		L I-VI	346.7 \pm 45.87	184.1 \pm 4.37	453.9 \pm 117.8	467.60 \pm 98.4	
Figure 5			Vehicle		CDPPB		
B	Homer1bc ⁺ puncta/100 μ m ²	LII-III	85.87 \pm 3.58	61.63 \pm 3.91	76.23 \pm 3.87	80.07 \pm 4.64	
		L V	72.37 \pm 3.43	51.10 \pm 4.78	71.49 \pm 3.95	67.31 \pm 5.18	
C	Clasping time (SEC)		0.00 \pm 0.00	10.61 \pm 2.38	0.00 \pm 0.00	5.36 \pm 1.76	
E	c-FOS intensity	L I-VI	1.48 \pm 0.22	0.88 \pm 0.06	1.09 \pm 0.26	1.05 \pm 0.6	
Figure 6			C1	P1	C2	P2	
B	Homer1bc ⁺ puncta/100 μ m ²		92.17	70.25	91.86	68.70	
C	PSD-95 ⁺ puncta/100 μ m ²		85.53	66.08	88.62	62.53	
D	VGluT1 ⁺ puncta/100 μ m ²		59.70	39.1	50.3	38.8	
F	PSD-95/Act		1.25	0.1	0.56	0.16	
G	Homer1bc/Act		1.45	0.47	0.76	0.16	
H	mGluR5/Act		0.85	0.65	0.33	0.08	

580 Table2. List of antibodies used

Primary Antibody	Species of origin	Working dilution			Supplier and catalog no.
		WB	IF	IP	
Homer1bc	Rabbit	1:1000	1:500		Synaptic System, Germany, cod. 160 023
Homer1bc	Mouse			1 mg	Santa Cruz Biotechnology, cod. sc-25271
mGluR5	Rabbit	1:500	1:250		Millipore, Germany, USA cod. AB5675
ARC	Rabbit		1:500		Synaptic System, Germany, cod. 156 003
c-FOS	Rabbit		1:1500		Santa Cruz Biotechnology, USA, cat. sc-52
PSD-95	Mouse	1:500	1:250		Neuromab; CA, USA, Clone K28/43
VGluT1	Guinea pig		1:5000		Millipore, Germany, cat. 5905

581

582

583 **Acknowledgments:**

584 **Author's contribution:** AG and MG conceived and designed the study. AG performed the
585 experiments. LL, GS, RM, EP performed IOS experiments. SG performed experiments on human
586 tissues, AG, RP, NM, FP performed behavioural experiments, AG, RP performed
587 immunofluorescence experiments. AM and GC performed electrophysiological experiments. CS, AN
588 synthesized and provided RO6807794; AG, RP, AR, TP, AM and MG analyzed the data. AG and
589 MG wrote the manuscript.

590 **Funding:** This work was supported by research grants from: University of Pennsylvania Orphan
591 Disease Center on behalf of LouLou Foundation (CDKL5 PILOT GRANT PROGRAM n. CDKL5 -
592 17 - 106 – 01) and from Associazione CDKL5 Insieme verso la cura (Italy) to MG and TP; The
593 International Foundation for CDKL5 Research, Associazione Albero di Greta and Fondazione CRT
594 (n. 2018.0889) and by Fondazione Telethon Grant (n. GGP15098) to MG.

595 **Institutional Review Board Statement:** The study was conducted in accordance with European
596 Community Council Directive 2010/63/UE for care and use of experimental animals with protocols
597 approved by the Italian Minister for Scientific Research (Authorization number 38/2020-PR) and the
598 Bioethics Committee of the University of Torino, Italy.

599 **Conflicts of Interest:** The authors do not have financial disclosures or conflict of interest to declare.

600

601

602

603

604

605 **References**

606 Aloisi E, Le Corf K, Dupuis J, Zhang P, Ginger M, Labrousse V, Spatuzza M, Georg Haberl
607 M, Costa L, Shigemoto R, Tappe-Theodor A, Drago F, Vincenzo Piazza P, Mulle C, Groc L, Ciranna
608 L, Catania MV, Frick A. 2017. Altered surface mGluR5 dynamics provoke synaptic NMDAR
609 dysfunction and cognitive defects in Fmr1 knockout mice. *Nat Commun* **8**:1103. doi:10.1038/s41467-
610 017-01191-2

611 Amendola E, Zhan Y, Mattucci C, Castroflorio E, Calcagno E, Fuchs C, Lonetti G, Silingardi
612 D, Vyssotski AL, Farley D, Ciani E, Pizzorusso T, Giustetto M, Gross CT. 2014. Mapping
613 pathological phenotypes in a mouse model of CDKL5 disorder. *PLoS One* **9**:5–16.
614 doi:10.1371/journal.pone.0091613

615 Ango F, Pin JP, Tu JC, Xiao B, Worley PF, Bockaert J, Fagni L. 2000. Dendritic and axonal
616 targeting of type 5 metabotropic glutamate receptor is regulated by Homer1 proteins and neuronal
617 excitation. *J Neurosci* **20**:8710–8716.

618 Auerbach BD, Osterweil EK, Bear MF. 2011. Mutations causing syndromic autism define an
619 axis of synaptic pathophysiology. *Nature* **480**:63–68. doi:10.1038/nature10658

620 Ballester-Rosado CJ, Sun H, Huang JY, Lu HC. 2016. mGluR5 exerts cell-autonomous
621 influences on the functional and anatomical development of layer IV cortical neurons in the mouse
622 primary somatosensory cortex. *J Neurosci* **36**:8802–8814. doi:10.1523/JNEUROSCI.1224-16.2016

623 Baltussen LL, Negraes PD, Silvestre M, Claxton S, Moeskops M, Christodoulou E, Flynn
624 HR, Snijders AP, Muotri AR, Ultanir SK. 2018. Chemical genetic identification of CDKL5 substrates
625 reveals its role in neuronal microtubule dynamics. *EMBO J* **37**:e99763.
626 doi:10.15252/embj.201899763

627 Barbiero I, Peroni D, Tramarin M, Chandola C, Rusconi L, Landsberger N, Kilstrup-Nielsen
628 C. 2017. The neurosteroid pregnenolone reverts microtubule derangement induced by the loss of a
629 functional CDKL5-IQGAP1 complex. *Hum Mol Genet* **26**:3520–3530. doi:10.1093/hmg/ddx237

630 Bellone C, Lüscher C, Mameli M. 2008. Mechanisms of synaptic depression triggered by
631 metabotropic glutamate receptors. *Cell Mol Life Sci* **65**:2913–2923. doi:10.1007/s00018-008-8263-3

632 Bertaso, F., Roussignol, G., Worley, P., Bockaert, J., Fagni, L., and Ango, F. (2010).

633 Homer1a-dependent crosstalk between NMDA and metabotropic glutamate receptors in mouse
634 neurons. *PLoS ONE* 5, e9755. doi:10.1371/journal.pone.0009755

635 Bouet V, Boulouard M, Toutain J, Divoux D, Bernaudin M, Schumann-Bard P, Freret T.
636 2009. The adhesive removal test: A sensitive method to assess sensorimotor deficits in mice. *Nat*
637 *Protoc* 4:1560–1564. doi:10.1038/nprot.2009.125

638 Chen C-C, Lu H-C, Brumberg JC. 2012. mGluR5 knockout mice display increased dendritic
639 spine densities. *Neurosci Lett* 524:65–68. doi:10.1016/J.NEULET.2012.07.014

640 Chen Y, Goudet C, Pin J-P, Conn PJ. 2008. N-{4-Chloro-2-[(1,3-dioxo-1,3-dihydro-2H-
641 isoindol-2-yl)methyl]phenyl}-2-hydroxybenzamide (CPPHA) acts through a novel site as a positive
642 allosteric modulator of group 1 metabotropic glutamate receptors. *Mol Pharmacol* 73:909–18.
643 doi:10.1124/mol.107.040097

644 Della Sala G, Putignano E, Chelini G, Melani R, Calcagno E, Michele Ratto G, Amendola E,
645 Gross CT, Giustetto M, Pizzorusso T. 2016. Dendritic Spine Instability in a Mouse Model of CDKL5
646 Disorder Is Rescued by Insulin-like Growth Factor 1. *Biol Psychiatry* 80:302–311.
647 doi:10.1016/j.biopsych.2015.08.028

648 Demarest S, Pestana-Knight EM, Olson HE, Downs J, Marsh ED, Kaufmann WE, Partridge
649 C-A, Leonard H, Gwadry-Sridhar F, Frame KE, Cross JH, Chin RFM, Parikh S, Panzer A,
650 Weisenberg J, Utley K, Jaksha A, Amin S, Khwaja O, Devinsky O, Neul JL, Percy AK, Benke TA.
651 2019. Severity Assessment in CDKL5 Deficiency Disorder. *Pediatr Neurol* 97:38–42.
652 doi:10.1016/J.PEDIATRNEUROL.2019.03.017

653 Demarest ST, Olson HE, Moss A, Pestana-Knight E, Zhang X, Parikh S, Swanson LC, Riley
654 KD, Bazin GA, Angione K, Niestroj L, Lal D, Juarez-Colunga E, Benke TA. 2019. CDKL5
655 deficiency disorder: Relationship between genotype, epilepsy, cortical visual impairment, and
656 development. *Epilepsia* 60:1733–1742. doi:10.1111/epi.16285

657 Edfawy M, Guedes JR, Pereira MI, Laranjo M, Carvalho MJ, Gao X, Ferreira PA, Caldeira
658 G, Franco LO, Wang D, Cardoso AL, Feng G, Carvalho AL, Peça J. 2019. Abnormal mGluR-
659 mediated synaptic plasticity and autism-like behaviours in Gprasp2 mutant mice. *Nat Commun*
660 10:1431. doi:10.1038/s41467-019-09382-9

661 Ferraguti, F., Shigemoto, R. Metabotropic glutamate receptors. *Cell Tissue Res* 326, 483–504

662 (2006). <https://doi.org/10.1007/s00441-006-0266-5>

663 Fuchs C, Trazzi S, Torricella R, Viggiano R, De Franceschi M, Amendola E, Gross C, Calz??
664 L, Bartesaghi R, Ciani E. 2014. Loss of CDKL5 impairs survival and dendritic growth of newborn
665 neurons by altering AKT/GSK-3?? signaling. *Neurobiol Dis* **70**:53–68.
666 doi:10.1016/j.nbd.2014.06.006

667 Giuffrida R, Musumeci S, D'Antoni S, Bonaccorso CM, Giuffrida-Stella AM, Oostra BA,
668 Catania MV. 2005. A reduced number of metabotropic glutamate subtype 5 receptors are associated
669 with constitutive Homer proteins in a mouse model of fragile X syndrome. *J Neurosci* **25**:8908–8916.
670 doi:10.1523/JNEUROSCI.0932-05.2005

671 Gogliotti RG, Senter RK, Rook JM, Ghoshal A, Zamorano R, Malosh C, Stauffer SR, Bridges
672 TM, Bartolome JM, Daniels JS, Jones CK, Lindsley CW, Conn PJ, Niswender CM. 2016. mGlu₅
673 positive allosteric modulation normalizes synaptic plasticity defects and motor phenotypes in a mouse
674 model of Rett syndrome. *Hum Mol Genet* **25**:1990–2004. doi:10.1093/hmg/ddw074

675 Grasso S, Chapelle J, Salemme V, Aramu S, Russo I, Vitale N, Verdun di Cantogno L,
676 Dallaglio K, Castellano I, Amici A, Centonze G, Sharma N, Lunardi S, Cabodi S, Cavallo F,
677 Lamolinara A, Stramucci L, Moiso E, Provero P, Albini A, Sapino A, Staaf J, Di Fiore PP, Bertalot
678 G, Pece S, Tosoni D, Confalonieri S, Iezzi M, Di Stefano P, Turco E, Defilippi P. The scaffold protein
679 p140Cap limits ERBB2-mediated breast cancer progression interfering with Rac GTPase-controlled
680 circuitries. *Nat Commun*. 2017 Mar 16;8:14797. doi: 10.1038/ncomms14797. Erratum in: *Nat*
681 *Commun*. 2018 Mar 30;9:16203. PMID: 28300085; PMCID: PMC5357316.

682 Guo W, Wei F, Zou S, Robbins MT, Sugiyama S, Ikeda T, Tu J-C, Worley PF, Dubner R, Ren
683 K. 2004. Group I metabotropic glutamate receptor NMDA receptor coupling and signaling cascade
684 mediate spinal dorsal horn NMDA receptor 2B tyrosine phosphorylation associated with
685 inflammatory hyperalgesia. *J Neurosci* **24**:9161–73. doi:10.1523/JNEUROSCI.3422-04.2004

686 Hering H, Sheng M. 2001. Dendritic spines: structure, dynamics and regulation. *Nat Rev*
687 *Neurosci* **2**:880–888. doi:10.1038/35104061

688 Kameshita I, Sekiguchi M, Hamasaki D, Sugiyama Y, Hatano N, Suetake I, Tajima S,
689 Sueyoshi N. 2008. Cyclin-dependent kinase-like 5 binds and phosphorylates DNA methyltransferase
690 1. *Biochem Biophys Res Commun* **377**:1162–1167. doi:10.1016/J.BBRC.2008.10.113

- 691 Kelly E, Schaeffer SM, Dhamne SC, Lipton JO, Lindemann L, Honer M, Jaeschke G, Super
692 CE, Lammers SH, Modi ME, Silverman JL, Dreier JR, Kwiatkowski DJ, Rotenberg A, Sahin M.
693 2018. mGluR5 Modulation of Behavioral and Epileptic Phenotypes in a Mouse Model of Tuberous
694 Sclerosis Complex. *Neuropsychopharmacology* **43**:1457–1465. doi:10.1038/npp.2017.295
- 695 Kinney GG, O'Brien JA, Lemaire W, Burno M, Bickel DJ, Clements MK, Chen T-B,
696 Wisnoski DD, Lindsley CW, Tiller PR, Smith S, Jacobson MA, Sur C, Duggan ME, Pettibone DJ,
697 Conn PJ, Williams DL. 2005. A novel selective positive allosteric modulator of metabotropic
698 glutamate receptor subtype 5 has in vivo activity and antipsychotic-like effects in rat behavioral
699 models. *J Pharmacol Exp Ther* **313**:199–206. doi:10.1124/jpet.104.079244
- 700 Komotar RJ, Kim GH, Sughrue ME, Otten ML, Rynkowski MA, Kellner CP, Hahn DK,
701 Merkow MB, Garrett MC, Starke RM, Connolly ES. 2007. Neurologic assessment of somatosensory
702 dysfunction following an experimental rodent model of cerebral ischemia. *Nat Protoc* **2**:2345–2347.
703 doi:10.1038/nprot.2007.359
- 704 Lujan R, Nusser Z, Roberts JD, Shigemoto R, Somogyi P. 1996. Perisynaptic location of
705 metabotropic glutamate receptors mGluR1 and mGluR5 on dendrites and dendritic spines in the rat
706 hippocampus. *Eur J Neurosci* **8**:1488–1500. doi:10.1111/j.1460-9568.1996.tb01611.x
- 707 Lupori L, Sagona G, Fuchs C, Mazziotti R, Stefanov A, Putignano E, Napoli D, Strettoi E,
708 Ciani E, Pizzorusso T. 2019. Site-specific abnormalities in the visual system of a mouse model of
709 CDKL5 deficiency disorder. *Hum Mol Genet* **28**:2851–2861. doi:10.1093/hmg/ddz102
- 710 Marcantoni A, Vandael DHF, Mahapatra S, Carabelli V, Sinnegger-Brauns MJ, Striessnig J,
711 Carbone E (2010): Loss of Cav1.3 Channels Reveals the Critical Role of L-Type and BK Channel
712 Coupling in Pacemaking Mouse Adrenal Chromaffin Cells. *J Neurosci*. **30**: 491–504.
- 713 Marcantoni A, Cerullo MS, Buxeda P, Tomagra G, Giustetto M, Chiantia G, Carabelli V,
714 Carbone E. Amyloid Beta42 oligomers up-regulate the excitatory synapses by potentiating
715 presynaptic release while impairing postsynaptic NMDA receptors. *J Physiol*. 2020
716 Jun;598(11):2183-2197. doi: 10.1113/JP279345. Epub 2020 May 14. PMID: 32246769.
- 717 Mari F, Azimonti S, Bertani I, Bolognese F, Colombo E, Caselli R, Scala E, Longo I, Grosso
718 S, Pescucci C, Ariani F, Hayek G, Balestri P, Bergo A, Badaracco G, Zappella M, Broccoli V, Renieri
719 A, Kilstrup-Nielsen C, Landsberger N. 2005. CDKL5 belongs to the same molecular pathway of
720 MeCP2 and it is responsible for the early-onset seizure variant of Rett syndrome. *Hum Mol Genet*

721 **14**:1935–1946. doi:10.1093/hmg/ddi198

722 Mazziotti R, Lupori L, Sagona G, Gennaro M, Sala G Della, Putignano E, Pizzorusso T. 2017.
723 Searching for biomarkers of CDKL5 disorder: early-onset visual impairment in CDKL5 mutant mice.
724 *Hum Mol Genet* **26**:2290–2298. doi:10.1093/hmg/ddx119

725 Mellone M, Stanic J, Hernandez LF, Iglesias E, Zianni E, Longhi A, Prigent A, Picconi B,
726 Calabresi P, Hirsch EC, Obeso JA, Di Luca M, Gardoni F. NMDA receptor GluN2A/GluN2B subunit
727 ratio as synaptic trait of levodopa-induced dyskinesias: from experimental models to patients. *Front*
728 *Cell Neurosci.* 2015 Jul 6;9:245. doi: 10.3389/fncel.2015.00245. PMID: 26217176; PMCID:
729 PMC4491616.

730 Ménard C, Quirion R. 2012. Successful cognitive aging in rats: A role for mGluR5 glutamate
731 receptors, homer 1 proteins and downstream signaling pathways. *PLoS One* **7**:e28666.
732 doi:10.1371/journal.pone.0028666

733 Moulton PR, Gladding CM, Sanderson TM, Fitzjohn SM, Bashir ZI, Molnar E, Collingridge
734 GL. 2006. Tyrosine phosphatases regulate AMPA receptor trafficking during metabotropic glutamate
735 receptor-mediated long-term depression. *J Neurosci* **26**:2544–2554. doi:10.1523/JNEUROSCI.4322-
736 05.2006

737 Muñoz IM, Morgan ME, Peltier J, Weiland F, Gregorczyk M, Cm Brown F, Macartney T,
738 Toth R, Trost M, Rouse J. 2018. Phosphoproteomic screening identifies physiological substrates of
739 the CDKL5 kinase. *EMBO J* **37**:e99559.

740 Nawaz MS, Giarda E, Bedogni F, La Montanara P, Ricciardi S, Ciceri D, Alberio T,
741 Landsberger N, Rusconi L, Kilstrup-Nielsen C. 2016. CDKL5 and Shootin1 Interact and Concur in
742 Regulating Neuronal Polarization. *PLoS One* **11**:e0148634. doi:10.1371/journal.pone.0148634

743 Negraes PD, Trujillo CA, Yu N-K, Wu W, Yao H, Liang N, Lautz JD, Kwok E, McClatchy
744 D, Diedrich J, de Bartolome SM, Truong J, Szeto R, Tran T, Herai RH, Smith SEP, Haddad GG,
745 Yates JR, Muotri AR. 2021. Altered network and rescue of human neurons derived from individuals
746 with early-onset genetic epilepsy. *Mol Psychiatry.* doi:10.1038/s41380-021-01104-2

747 Oh WC, Hill TC, Zito K. 2013. Synapse-specific and size-dependent mechanisms of spine
748 structural plasticity accompanying synaptic weakening. *Proc Natl Acad Sci U S A* **110**:E305-12.
749 doi:10.1073/pnas.1214705110

- 750 Okuda K, Kobayashi S, Fukaya M, Watanabe A, Murakami T, Hagiwara M, Sato T, Ueno H,
751 Ogonuki N, Komano-Inoue S, Manabe H, Yamaguchi M, Ogura A, Asahara H, Sakagami H,
752 Mizuguchi M, Manabe T, Tanaka T. 2017. CDKL5 controls postsynaptic localization of GluN2B-
753 containing NMDA receptors in the hippocampus and regulates seizure susceptibility. *Neurobiol Dis*
754 **106**:157–170. doi:10.1016/j.nbd.2017.07.002
- 755 Perroy J, Raynaud F, Homburger V, Rousset M-C, Telley L, Bockaert JL, Fagni L. 2008.
756 Direct Interaction Enables Cross-talk between Ionotropic and Group I Metabotropic Glutamate
757 Receptors. *J Biol Chem* **283**:6799–805. doi:10.1074/jbc.M705661200
- 758 Piers TM, Kim DH, Kim BC, Regan P, Whitcomb DJ, Cho K. 2012. Translational concepts
759 of mglur5 in synaptic diseases of the brain. *Front Pharmacol* **3** NOV:1–7.
760 doi:10.3389/fphar.2012.00199
- 761 Pizzo R, Gurgone A, Castroflorio E, Amendola E, Gross C, Sassoè-Pognetto M, Giustetto M.
762 2016. Lack of Cdkl5 Disrupts the Organization of Excitatory and Inhibitory Synapses and
763 Parvalbumin Interneurons in the Primary Visual Cortex. *Front Cell Neurosci* **10**:261.
764 doi:10.3389/fncel.2016.00261
- 765 Pizzo R, Lamarca A, Sassoè-Pognetto M, Giustetto M. 2019. Structural Bases of Atypical
766 Whisker Responses in a Mouse Model of CDKL5 Deficiency Disorder. *Neuroscience* **95**.
767 doi:10.1016/j.neuroscience.2019.08.033
- 768 Reiner A, Levitz J. 2018. Glutamatergic Signaling in the Central Nervous System: Ionotropic
769 and Metabotropic Receptors in Concert. *Neuron* **98**:1080–1098.
770 doi:10.1016/J.NEURON.2018.05.018
- 771 Ricciardi S, Ungaro F, Hambrock M, Rademacher N, Stefanelli G, Brambilla D, Sessa A,
772 Magagnotti C, Bachi A, Giarda E, Verpelli C, Kilstrup-Nielsen C, Sala C, Kalscheuer VM, Broccoli
773 V. 2012. CDKL5 ensures excitatory synapse stability by reinforcing NGL-1-PSD95 interaction in the
774 postsynaptic compartment and is impaired in patient iPSC-derived neurons. *Nat Cell Biol* **14**:911–23.
775 doi:10.1038/ncb2566
- 776 Ronesi JA, Collins KA, Hays SA, Tsai N-P, Guo W, Birnbaum SG, Hu J-H, Worley PF,
777 Gibson JR, Huber KM. 2012. Disrupted Homer scaffolds mediate abnormal mGluR5 function in a
778 mouse model of fragile X syndrome. *Nat Neurosci* **15**:431–40, S1. doi:10.1038/nn.3033

779 Rusconi L, Salvatoni L, Giudici L, Bertani I, Kilstrup-Nielsen C, Broccoli V, Landsberger N.
780 2008. CDKL5 expression is modulated during neuronal development and its subcellular distribution
781 is tightly regulated by the C-terminal tail. *J Biol Chem* **283**:30101–11. doi:10.1074/jbc.M804613200

782 Sala C, Futai K, Yamamoto K, Worley PF, Hayashi Y, Sheng M. 2003. Inhibition of Dendritic
783 Spine Morphogenesis and Synaptic Transmission by Activity-Inducible Protein Homer1a. *J Neurosci*
784 **23**:6327–6337. doi:23/15/6327 [pii]

785 Scheefhals N, MacGillavry HD. 2018. Functional organization of postsynaptic glutamate
786 receptors. *Mol Cell Neurosci* **91**:82–94. doi:10.1016/J.MCN.2018.05.002

787 Shiraishi-Yamaguchi Y, Furuichi T. The Homer family proteins. *Genome Biol.*
788 2007;8(2):206. doi: 10.1186/gb-2007-8-2-206. PMID: 17316461; PMCID: PMC1852408.

789 Tomassy GS, Morello N, Calcagno E, Giustetto M. Developmental abnormalities of cortical
790 interneurons precede symptoms onset in a mouse model of Rett syndrome. *J Neurochem.* 2014
791 Oct;131(1):115-27. doi: 10.1111/jnc.12803. Epub 2014 Aug 5. PMID: 24978323.

792 Tramarin M, Rusconi L, Pizzamiglio L, Barbiero I, Peroni D, Scaramuzza L, Guilliams T,
793 Cavalla D, Antonucci F, Kilstrup-Nielsen C. 2018. The antidepressant tianeptine reverts synaptic
794 AMPA receptor defects caused by deficiency of CDKL5. *Hum Mol Genet* **27**:2052–2063.
795 doi:10.1093/hmg/ddy108

796 Trazzi S, Fuchs C, Viggiano R, De Franceschi M, Valli E, Jedynak P, Hansen FK, Perini G,
797 Rimondini R, Kurz T, Bartesaghi R, Ciani E. 2016. HDAC4: a key factor underlying brain
798 developmental alterations in CDKL5 disorder. *Hum Mol Genet* **25**:3887–3907.
799 doi:10.1093/hmg/ddw231

800 Trazzi S, De Franceschi M, Fuchs C, Bastianini S, Viggiano R, Lupori L, Mazziotti R, Medici
801 G, Lo Martire V, Ren E, Rimondini R, Zoccoli G, Bartesaghi R, Pizzorusso T, Ciani E. CDKL5
802 protein substitution therapy rescues neurological phenotypes of a mouse model of CDKL5 disorder.
803 *Hum Mol Genet.* 2018 May 1;27(9):1572-1592. doi: 10.1093/hmg/ddy064. PMID: 29474534.

804 Tu JC, Xiao B, Naisbitt S, Yuan JP, Petralia RS, Brakeman P, Doan A, Aakalu VK, Lanahan
805 AA, Sheng M, Worley PF. 1999. Coupling of mGluR/Homer and PSD-95 Complexes by the Shank
806 Family of Postsynaptic Density Proteins. *Neuron* **23**:583–592.

807 van Brussel, L., Gerits, A., and Arckens, L. (2009). Identification and localization of

808 functional subdivisions in the visual cortex of the adult mouse. *J. Comp. Neurol.* 514, 107–116. doi:
809 10.1002/cne.21994

810 Verpelli C, Dvoretzkova E, Vicidomini C, Rossi F, Chiappalone M, Schoen M, Di Stefano B,
811 Mantegazza R, Broccoli V, Böckers TM, Dityatev A, Sala C. 2011. Importance of Shank3 protein in
812 regulating metabotropic glutamate receptor 5 (mGluR5) expression and signaling at synapses. *J Biol*
813 *Chem* **286**:34839–50. doi:10.1074/jbc.M111.258384

814 Vicidomini C, Ponzoni L, Lim D, Schmeisser M, Reim D, Morello N, Orelanna D, Tozzi A,
815 Durante V, Scalmani P, Mantegazza M, Genazzani AA, Giustetto M, Sala M, Calabresi P, Boeckers
816 TM, Sala C, Verpelli C. 2017. Pharmacological enhancement of mGlu5 receptors rescues behavioral
817 deficits in SHANK3 knock-out mice Europe PMC Funders Group. *Mol Psychiatry* **22**:689–702.

818 Wang H, Zhuo M. 2012. Group I metabotropic glutamate receptor-mediated gene
819 transcription and implications for synaptic plasticity and diseases. *Front Pharmacol* **3**:189.
820 doi:10.3389/fphar.2012.00189

821 Wang I-TJ, Allen M, Goffin D, Zhu X, Fairless AH, Brodtkin ES, Siegel SJ, Marsh ED, Blendy
822 JA, Zhou Z. 2012. Loss of CDKL5 disrupts kinome profile and event-related potentials leading to
823 autistic-like phenotypes in mice. *Proc Natl Acad Sci U S A* **109**:21516–21.
824 doi:10.1073/pnas.1216988110

825 Yennawar M, White RS, Jensen FE. 2019. Neurobiology of Disease AMPA Receptor
826 Dysregulation and Therapeutic Interventions in a Mouse Model of CDKL5 Deficiency Disorder.
827 doi:10.1523/JNEUROSCI.2041-18.2019

828 Zhu Y-C, Li D, Wang L, Lu B, Zheng J, Zhao S-L, Zeng R, Xiong Z-Q. 2013. Palmitoylation-
829 dependent CDKL5-PSD-95 interaction regulates synaptic targeting of CDKL5 and dendritic spine
830 development. *Proc Natl Acad Sci U S A* **110**:9118–23. doi:10.1073/pnas.1300003110

831

832 **Figure legends**

833 **Figure 1. CDKL5 loss is responsible for both the disruption of mGluR5-Homer1bc interaction**
834 **and the reduction of mGluR5 localization in the cortical neuropil. (A)** Co-IP of cortical
835 synaptosomal fraction (P2) from P56 mice by using anti-Homer1bc. IgG: control lane in the absence
836 of antibodies. Immunoprecipitates and inputs were analyzed by immunoblotting for mGluR5 and
837 Homer1bc. **(B)** Bar graphs showing Co-IP quantitation expressed as optical density (O.D.). **(C)**
838 Confocal microscopy images showing mGluR5⁺ (green) and PSD-95⁺ (red) immunopuncta in layers
839 II/III of S1 cortex (scale bar: 5 μm). **(D)** Bar graphs displaying the density of mGluR5⁺ puncta.
840 Student T test *p < 0.05 (Co-IP: n = 8 IFL: n = 4).

841

842 **Figure 2. CDKL5 loss tampers with both mEPSCs and mGluR5-induced NMDA current.**

843 **(A)** Sample traces of miniature excitatory postsynaptic current (mEPSC) recorded from Cdk15^{+y}
844 neurons **(A, upper part)** and Cdk15^{-y} neurons **(B, upper part)** and after the application of DHPG
845 **(A, B lower part)**. **(C-D)** Bar graphs showing the mean average amplitude **(C)** and the inter-event
846 interval (IEI) of mEPSCs **(D)**. **(E)** Bar graphs displaying the % change of IEI after the application of
847 DHPG (100 μM). **(F)** Representative traces of currents obtained with patch-clamp recordings on S1
848 neurons cultures from Cdk15^{+y} and Cdk15^{-y} embryos after NMDA (50 μM) application **(upper part)**,
849 bar graphs showing differences of I_{NMDA} current between genotypes **(lower part)**. **(G)** Representative
850 traces of NMDA currents on S1 neurons after 2-min application of DHPG (100 μM-**upper part**); bar
851 graphs showing the % change of I_{NMDA} after the application of DHPG **(lower part)**. **(H)**
852 Representative traces of NMDA after 2-min CDPPB + NMDA application **(upper part)**, bar graphs
853 showing the % change of I_{NMDA} current after the application of CDPPB **(lower part)**. Student's t-
854 test, chi-square, two-way ANOVA followed by Fisher's multiple comparison test, * p < 0.05, ** p <
855 0.01, *** p < 0.001 (mEPSC Cdk15^{+y} n = 22 cells, Cdk15^{-y} n = 28; minis+DHPG: n = 12 cells.
856 NMDA: Cdk15^{+y} n = 36 cells, Cdk15^{-y} n = 23 cells; NMDA+DHPG Cdk15^{+y} n = 15 cells and

857 NMDA+DHPG Cdk15^{-y} n = 14 cells; NMDA+CDPPB Cdk15^{+y} n = 12 cells; NMDA+CDPPB Cdk15^{-y}
858 ^y n = 9 cells).

859

860 **Figure 3. Acute CDPPB treatment rescues CVI, sensorimotor and memory deficits in Cdk15^{-y}**

861 **mice. (A)** Samples images showing differences of IOS evoked responses in vehicle- and CDPPB-

862 treated Cdk15^{-y} mice. **(B)** Trajectory of the IOS amplitude in vehicle-Cdk15^{+y}, vehicle-Cdk15^{+y} and

863 CDPPB-Cdk15^{-y} treated mice. **(C)** Bar graphs showing contact latency with the tape placed under

864 mice's forepaw. **(D, E)** Bar graphs showing the percentage of the correct alternations **(D)** and the

865 number of entries **(E)** made by Cdk15^{+y} and Cdk15^{-y} mice, treated with either vehicle or CDPPB, in

866 the Y-maze. Two-way ANOVA followed by Sidak or Bonferroni's multiple comparison test, * p<

867 0.05, ** p< 0.01 (IOS: vehicle-Cdk15^{+y} n = 3, vehicle-Cdk15^{-y} n = 8, CDPPB-Cdk15^{-y} n = 6;

868 behavioural tests: vehicle-Cdk15^{+y} n = 12, vehicle-Cdk15^{-y} n = 13, CDPPB-Cdk15^{+y} n = 8, CDPPB-

869 Cdk15^{-y} n = 7).

870

871 **Figure 4. Structural defects exhibited by Cdk15^{-y} mice cortices are rescued by an acute CDPPB**

872 **injection. (A, C)** Representative confocal images showing Homer1bc⁺ and mGluR5⁺ puncta in layer

873 II-III of S1 cortex from either vehicle- or CDPPB-treated mice (scale bar: 5 μm). **(B, D)** Bar graphs

874 showing both Homer1bc⁺ **(B)** and mGluR5⁺ **(D)** immunopuncta density in layers II-III and V of both

875 S1 and V1 cortices in either vehicle- or CDPPB-treated mice. **(E)** Confocal images of ARC

876 immunostaining on coronal sections of the V1 cortex from mice treated with vehicle or CDPPB (scale

877 bar: 25 μm), and relative ARC⁺ cells density quantitation **(F)** throughout the cortical layers. Two-

878 way ANOVA followed by Fisher's multiple comparison test, *p < 0.05, ** p < 0.01, *** p < 0.001;

879 (n = 6 animals for each genotype).

880

881

882 **Figure 5. The subchronic treatment with CDPPB produces lasting effects in Cdk15^{-y} mice.**

883 (A) Representative confocal images of Homer1bc⁺ (red) immunofluorescence in layers II-III of the
884 S1 cortex. (B) Bar graphs showing Homer1bc⁺ puncta density in layers II-III and V of the S1 cortex
885 of either vehicle- and CDPPB-treated mice. (C) Bar graphs showing time spent clasping in vehicle-
886 and CDPPB-treated mice. (D) Representative images of c-Fos immunoreactive cells in S1 of vehicle-
887 and CDPPB-treated mice (scale bar 50 μ m). (E) Bar graphs showing the integrated intensity analysis
888 of c-Fos immunofluorescence in the S1 of vehicle- or CDPPB-treated mice. Two-way ANOVA
889 followed by Fisher's LSD: * $p < 0.05$, ** $p < 0.01$, *** $p < 0.001$ (Homer1bc⁺ puncta: $n = 9$ for each
890 group; clasping and c-Fos vehicle-Cdk15^{+y} $n = 34$, vehicle-Cdk15^{-y} $n = 23$, CDPPB-Cdk15^{+y} $n = 17$,
891 CDPPB-Cdk15^{-y} $n = 23$).

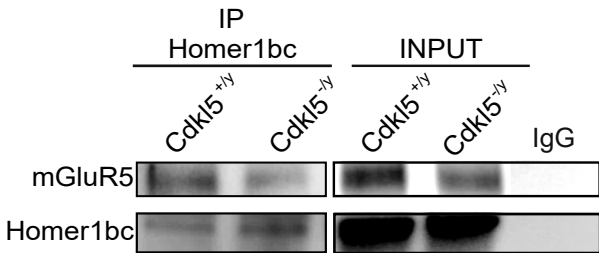
892

893 **Figure 6. Aberrant expression of excitatory synaptic proteins in the BA17 cortex of CDD**

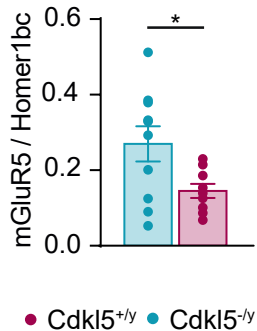
894 **patients.** (A) Illustrative confocal images taken from layers II-III of the BA17 cortex. (A) PSD-
895 95⁺(red), Homer1bc⁺(green), VGluT1⁺(green) immunofluorescence puncta. Note the virtually
896 complete overlapping of PSD-95 and Homer1bc immunofluorescence (scale bar: 5 μ m). (B, C, D)
897 Bar graphs showing the analysis of puncta density in layers II-III of BA17 cortices. (E) Western
898 blotting showing the expression of PSD95, Homer1bc and mGluR5 in lysates from BA17 cortices.
899 (F-H) Bar graphs displaying the optical density (O.D.) analysis of PSD95 (F), Homer1bc (G) and
900 mGluR5 (H) expression. Student's t-test, * $p < 0.05$, ** $p < 0.01$ (C1 = F, 4 years old; P1 = F, 5.7
901 years old; C2 = F, 29 years old; P2 = F, 30 years old).

Figure 1

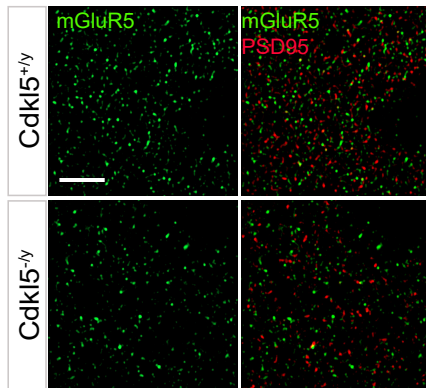
A



B



C



D

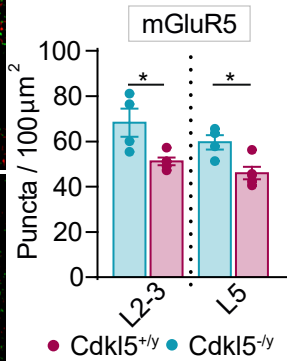


Figure 2

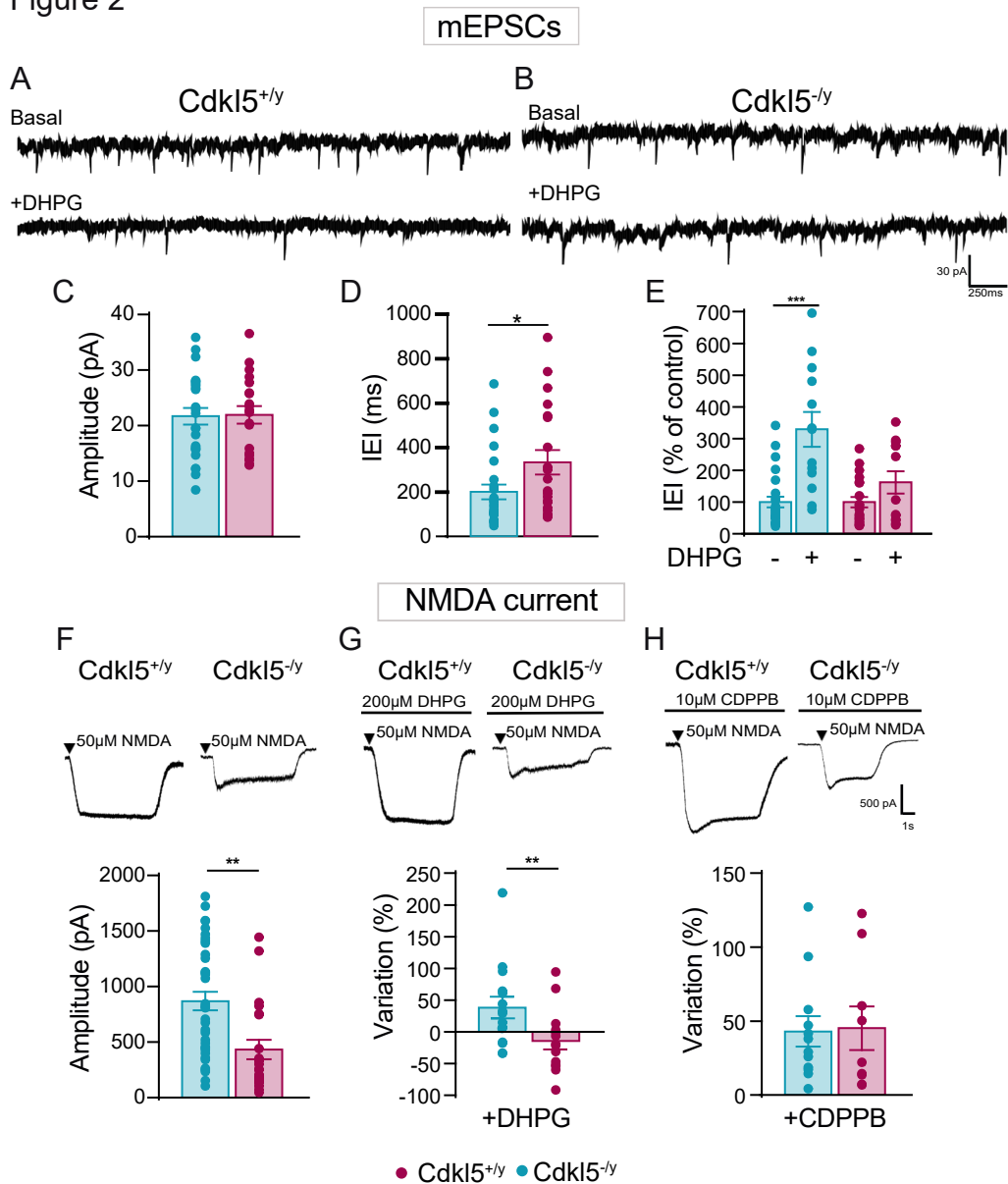


Figure 3

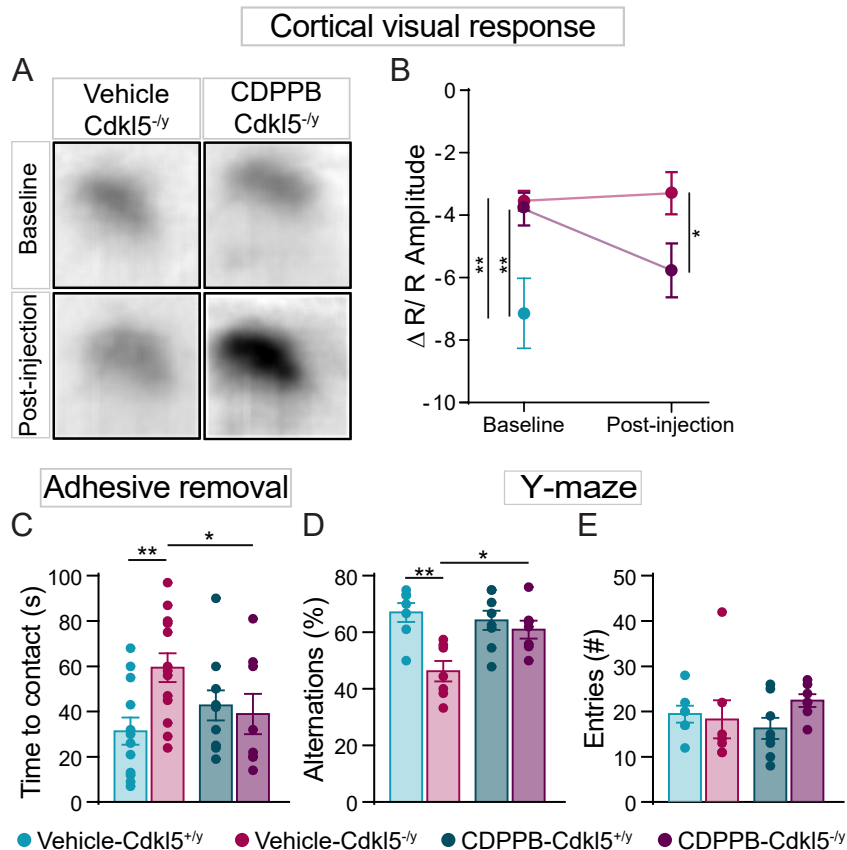


Figure 4

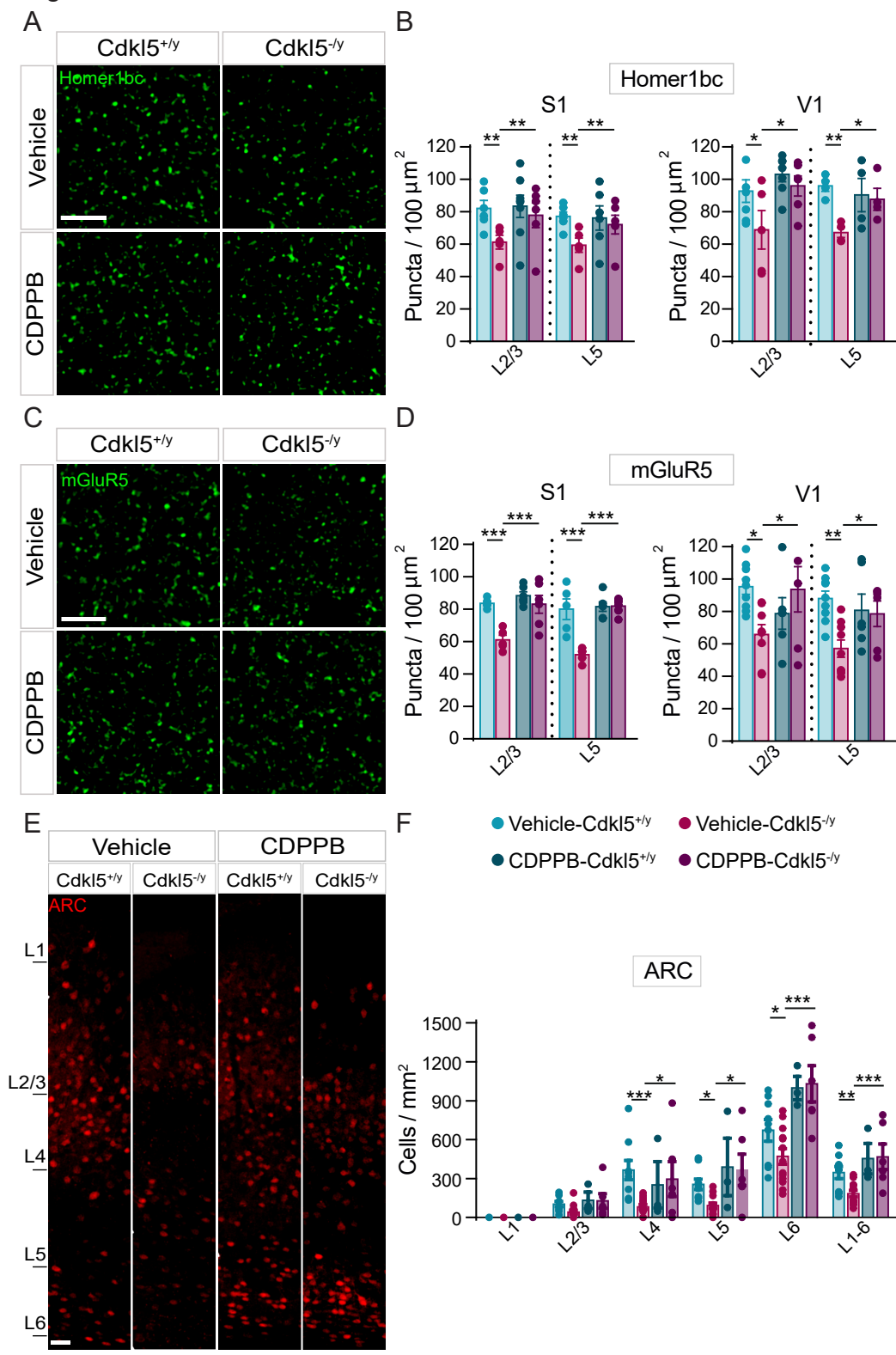


Figure 5

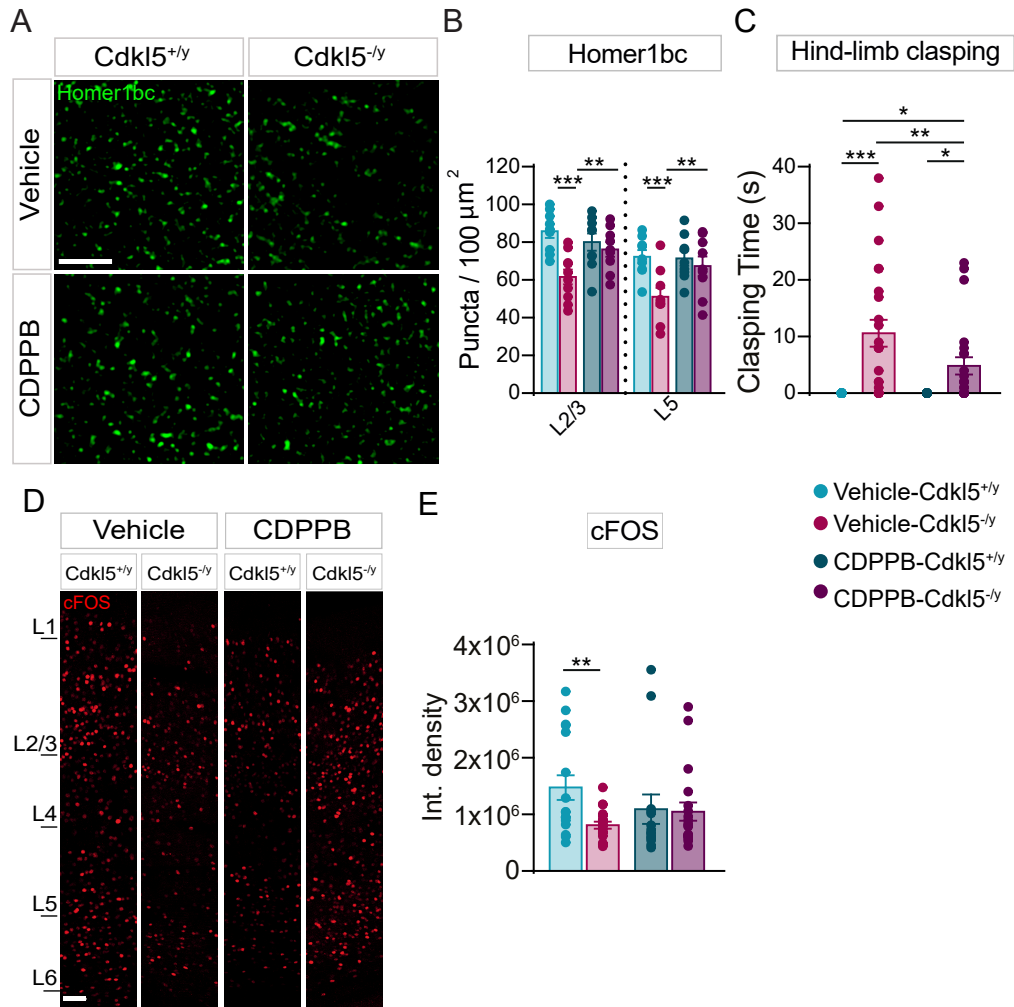
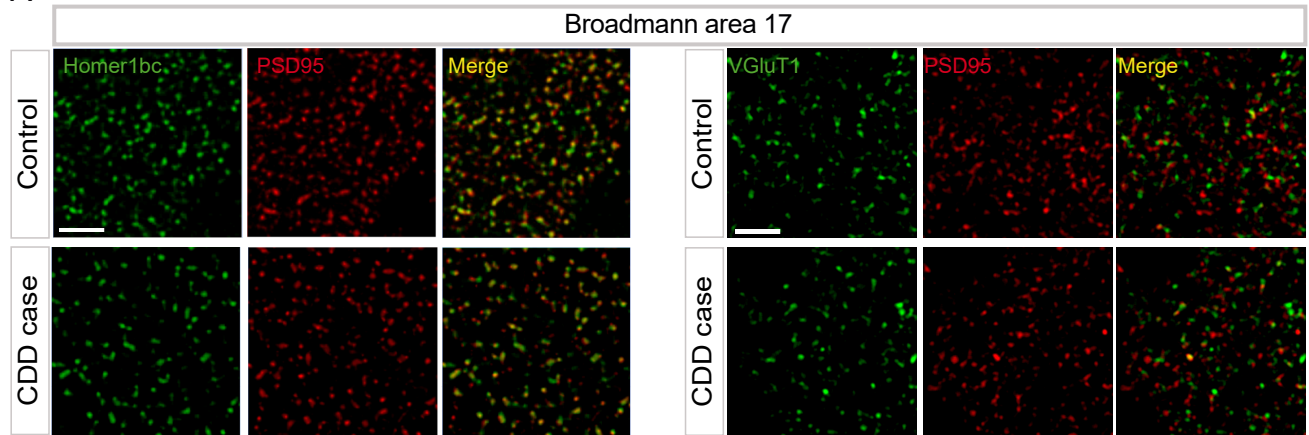
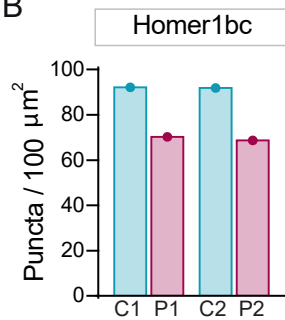


Figure 6

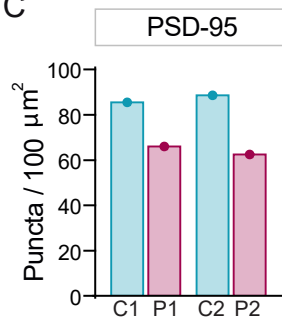
A



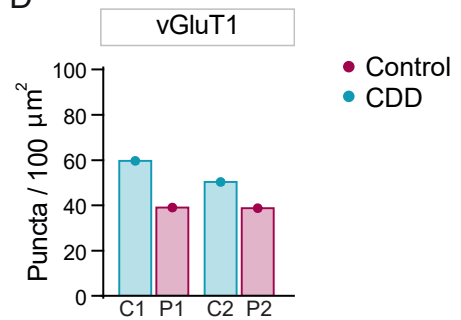
B



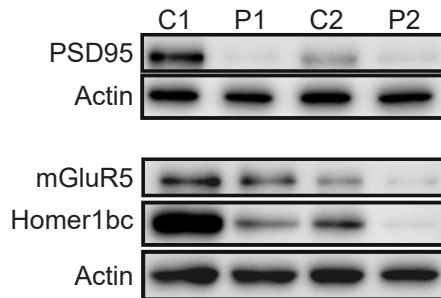
C



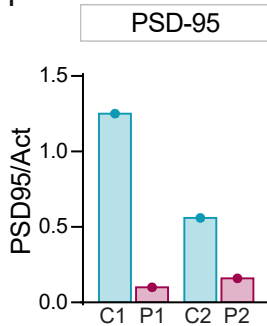
D



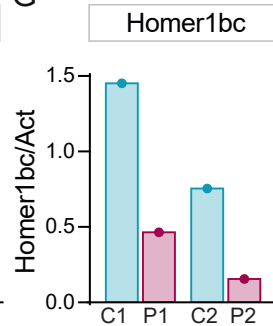
E



F



G



H

